SCIENCE CHINA
Information Sciences

• RESEARCH PAPER •

September 2025, Vol. 68, Iss. 9, 192301:1–192301:17
https://doi.org/10.1007/s11432-024-4417-y

Fundamental channel coupling effects for integrated sensing and communication systems

Xu GAN[1,2], Chongwen HUANG[1,2*], Zhaohui YANG[1], Xiaoming CHEN[1], Fan LIU[3], Zhaoyang ZHANG[1], Chau YUEN[4], Yong Liang GUAN[4] & Mérouane DEBBAH[5]

[1]*College of Information Science and Electronic Engineering, Zhejiang University, Hangzhou 310027, China*
[2]*State Key Laboratory of Integrated Service Networks, Xidian University, Xi'an 710071, China*
[3]*National Mobile Communications Research Laboratory, Southeast University, Nanjing 210096, China*
[4]*School of Electrical and Electronics Engineering, Nanyang Technological University, Singapore 639798, Singapore*
[5]*Center for 6G Technology, Khalifa University of Science and Technology, Abu Dhabi 127788, UAE*

Received 30 September 2024/Revised 13 February 2025/Accepted 24 April 2025/Published online 24 July 2025

Abstract Integrated sensing and communication (ISAC) has emerged as a promising solution to achieve high-rate communication and ultra-precise sensing for next-generation technologies. Existing studies primarily focus on trade-offs arising from communication and sensing (C&S) functions competing for shared system resources, while often overlooking coupling effects due to the co-location of communication users, sensing targets, and the base station, along with joint channel characteristics. To bridge this gap, we establish a novel framework for analyzing uplink and downlink ISAC performance, accounting for both trade-offs and coupling constraints. Specifically, we first investigate trade-offs through C&S performance regions between the channel estimation error and the successful detection probability in the uplink process, as well as between the transmission rate and Cramér-Rao lower bound in the downlink process. We derive theoretical formulations for these metrics and explore their scaling laws, asymptotic behaviors, and monotonicity properties. Additionally, the fundamental coupling effects can be examined by the joint ISAC coverage probability using stochastic geometry, which evaluates the likelihood of C&S simultaneously meeting performance thresholds. Our theoretical results provide innovative union bounds for ISAC systems, offering deep insights into the best achievable performance of one function under the coupling constraints inherently imposed by the other function. Finally, numerical results verify the accuracy of all theoretical derivations, and highlight the impact of trade-offs and coupling constraints on C&S performance regions.

Keywords integrated sensing and communication (ISAC), coupling effects, trade-offs, fundamental limits, stochastic geometry

Citation Gan X, Huang C W, Yang Z H, et al. Fundamental channel coupling effects for integrated sensing and communication systems. Sci China Inf Sci, 2025, 68(9): 192301, https://doi.org/10.1007/s11432-024-4417-y

1 Introduction

Integrated sensing and communication (ISAC) [1] introduces an innovative paradigm by integrating sensing capabilities into traditional communication systems, enabling beyond fifth-generation (B5G) and sixth-generation (6G) wireless networks [2] to support built-in communications and ultra-precise sensing [3,4]. It is anticipated to enhance communication and sensing (C&S) performance by leveraging shared system resources, and is recognized as a key enabler for emerging wireless scenarios. Consequently, the rapid development of ISAC is in urgent need of brand new technical solutions and analytical methods, which are currently gaining widespread attention in both academia and industry [5–9]. This has driven extensive research on ISAC across a broad range of areas, including waveform design [6], beamforming strategies [7], and advanced signal processing techniques [8, 9].

Among various enabling technologies, the resource trade-offs between C&S functions serve as key guidelines for system design. For instance, the work in [10] formulated an optimization problem to minimize the transmit power at the base station (BS) while ensuring a performance trade-off between the minimum probability of successful detection and the communication users' achievable rate. In [11], authors investigated the trade-off between the estimation Cramér-Rao lower bound (CRLB) for sensing and date rate for communication by optimizing the transmit power to maximize the transmission rate

* Corresponding author (email: chongwenhuang@zju.edu.cn)

under maximum CRLB constraint. Furthermore, Ref. [12] optimized the transmit power of each signal path to maximize the communication rate while maintaining constraints on sensing performance, and investigated the trade-off between the non-line-of-sight exploitation and reduction. These studies have proposed the allocation schemes to reach the boundary of achievable regions by solving optimization problems.

However, these system-specific design solutions lack a fundamental understanding of C&S in terms of resource utilization and fail to provide general insights or guidelines for achieving efficient ISAC systems. Fortunately, the underlying trade-offs are being progressively explored in depth [13–16]. In [13], the deterministic-random trade-off and corresponding Pareto boundaries were derived to characterize the two corner points of C&S performance, i.e., the maximum communication rate under the minimum CRLB and the minimum CRLB under the maximum communication rate. In [14], the authors derived the theoretical relationship among frequency domain subcarrier, time domain sensing symbols, and the CRLB to provide time-frequency resource distribution. Additionally, Ref. [15] holistically investigated both the time-frequency and spatial trade-offs by selecting the modulation order for data transmission and optimizing beamforming designs. Moreover, Ref. [16] proposed a new framework to evaluate the C&S using the communication and sensing mutual information, which served as performance metrics to achieve the trade-offs between C&S.

Still, the coexistence of C&S functions not only poses resource trade-off challenges but also introduces mutual coupling effects due to shared channel parameters, such as the locations of the BS, communication users (CUs), sensing targets (STs), and the fading coefficients between them. The channel coupling effects prevent C&S performance from independent analysis and design. Therefore, advancing ISAC services requires considering both trade-offs and coupling effects for optimal resource allocation schemes, however, which is little studied in current research. In particular, Ref. [17] considered the coupling between transmitted dual-function signals and corresponding echo signals as C&S mutual interference. On the other hand, Ref. [18] designed the reconfigurable intelligent surface (RIS)-assisted ISAC systems to strengthen the coupling level between C&S channels and achieve more performance gains from the joint design of ISAC signals. To provide more general insights into channel coupling effects on C&S performance, we utilize the joint coverage probability of dual functions as the unified performance metric. In fact, our previous studies have explored this area and produced preliminary results. Specifically, the work in [19] presented fundamental limits for the coverage and rate analysis of the ISAC performance, taking into account the coupling effects of dual functions in coexistence networks. Further, Ref. [20] investigated the RIS-assisted ISAC networks and examined the impact of distributed RIS locations on C&S coupling performance. Innovatively, these studies derived the joint ISAC coverage rate as the unified performance metric considering inherent trade-offs and coupling effects, which inspires further research on fundamental limits for ISAC systems.

This paper builds on this foundation to derive theoretical formulations for inherent performance constraint limits that exist between C&S due to channel coupling effects. Specifically, we first investigate trade-offs through C&S performance regions between the channel estimation normalized mean squared error (NMSE) and the successful detection probability in the uplink process, as well as between the communication sum-rate and sum-root-CRLB in the downlink process. The theoretical analysis for these metrics yields valuable insights into scaling laws, asymptotic behaviors, and monotonicity properties of ISAC performance. Furthermore, we define and derive the analytical formulations for the joint ISAC coverage, which evaluates the probability that C&S performance simultaneously exceeds the predefined thresholds. Consequently, the union bounds of C&S performance can be established through theoretical results of the joint ISAC coverage, which characterize the best achievable performance under coupling constraints. The main results and contributions of this paper are listed as follows.

(1) The differences between the uplink and downlink ISAC analysis focus on the various performance metrics. In particular, we model the uplink and downlink ISAC framework by seamlessly embedding sensing functions into the time division duplexing mode of the 3GPP 5G NR standards [21] without complex modifications to the pre-existing communication infrastructures. Specifically in the uplink process, the BS performs channel estimation for CUs while transmitting pilot sequences and utilizing echoes for target detection. During the subsequent downlink process, the BS transmits dual-function beams for simultaneous data transmission to CUs and parameter estimation of STs. Based on this framework, we investigate trade-offs through the achievable C&S performance regions between the channel estimation NMSE and the successful detection probability, as well as between the communication sum-rate and sensing sum-root-CRLB. These derived results reveal linear scaling laws between the transmit power of

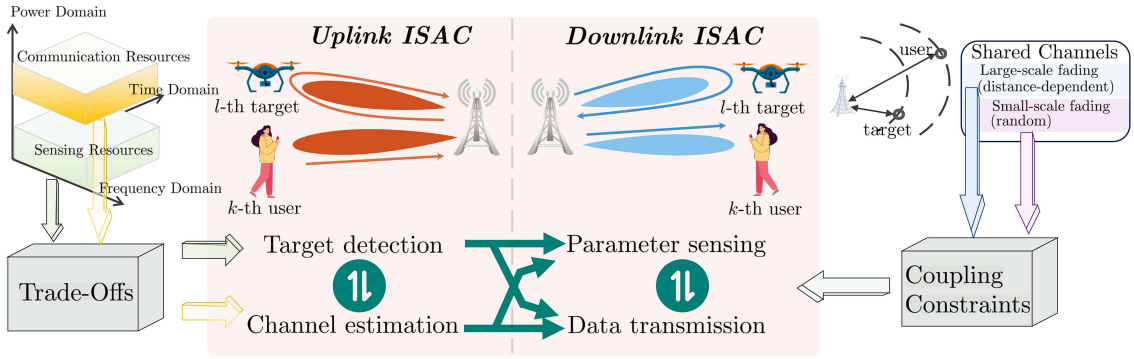

Figure 1 (Color online) Illustration of the considered ISAC systems.

the CUs and STs, and between the density of the CU distribution and the squared density of the ST distribution.

(2) Next, we utilize stochastic geometry tools to model the locations of the BS, CUs, and STs, which determine the large-scale fading coefficients. Combined with random small-scale fadings, these factors jointly influence C&S performance and impose inherent channel coupling effects. To address this issue, we define the joint ISAC coverage, which characterizes a unified metric to evaluate the performance of both C&S. By analyzing theoretical results for the joint ISAC coverage, we derive the union bound of C&S performance, which represents the best achievable performance bound of one function under the constraints of the other. This boundary offers deeper insights into the coupling constraints inherent in ISAC systems.

(3) Finally, we provide numerical results to validate the accuracy of the derived theoretical limits on the trade-offs and coupling effects for uplink and downlink ISAC performance. The simulations illustrate the impacts of key system parameters, such as transmit power and distribution density of CUs and STs, the number of BS antennas and the Rician factor, on the C&S performance regions. These results also reveal their scaling laws, asymptotic behaviors, and monotonicity properties. Moreover, the plotted joint ISAC coverage offers a clear depiction of fundamental coupling constraints through analytical union bounds.

2 System model

We consider an ISAC multiple input multiple output (MIMO) system, where an N-antenna BS simultaneously serves K CUs and senses L device-free targets over the same time-frequency resources. As depicted in Figure 1 within each coherent interval, T_u symbols are allocated for user channel estimation and target detection during the uplink ISAC process, while T_d symbols are dedicated to user data transmission and target parameter sensing in the downlink ISAC process. In this unified system, the C&S functions interact with each other in a coupling and trade-off manner. To explore their properties, we first introduce the channel model and network topology.

With the increase in system operating frequency, the channel model tends to have a deterministic line-of-sight (LoS) path in the scattering environment. Let $\boldsymbol{h}_k \in \mathbb{C}^{N\times 1}$ denote the channel from the k-th CU to the BS, following [22, 23] as $\boldsymbol{h}_k = \sqrt{\frac{\beta_{u,k}\kappa_{u,k}}{1+\kappa_{u,k}}}\bar{h}_k + \sqrt{\frac{\beta_{u,k}}{1+\kappa_{u,k}}}\tilde{h}_k$, where $\beta_{u,k} = C_0 d_{U,k}^{-\alpha}$ denotes the large-scale fading with C_0, $d_{u,k}$, and α being the path-loss coefficient at the reference distance 1 m, the distance between the k-th CU and the BS, and the path-loss exponential coefficient, respectively. Specifically, C_0 and α can be considered constants that depend on the physical properties of the environment. $\bar{h}_k$ accounts for the LoS component, and $\tilde{h}_k$ follows $\mathcal{CN}(\boldsymbol{0}, \boldsymbol{I}_N)$. $\kappa_{u,k}$ is the Rician factor denoting the power ratio between $\bar{h}_k$ and $\tilde{h}_k$. For notational convenience, let $\mu_k = \frac{\beta_{u,k}}{1+\kappa_{u,k}}$, such that $\boldsymbol{h}_k = \sqrt{\mu_k\kappa_{u,k}}\bar{h}_k + \sqrt{\mu_k}\tilde{h}_k$. In practice, $\bar{h}_k$ usually maintains constant for sufficient large intervals to be accurately estimated at the BS. Therefore, it can be assumed that $\bar{h}_k$ is perfectly known a priori in the communication theory.

Simultaneously, the BS senses targets with LoS channels from echo signals. Specifically, let $\boldsymbol{G}_l \in \mathbb{C}^{N\times N}$ denote the composite channel from the BS to the l-th ST and then back to the BS, such as $\boldsymbol{G}_l = \sqrt{\beta_{t,l}}\zeta_l \boldsymbol{a}_N(\theta_l)\boldsymbol{a}_N^{\mathrm{H}}(\theta_l)$, where $\beta_{t,l} = C_0 d_{T,l}^{-2\alpha}$ and $\zeta_l \sim \mathcal{CN}(0,1)$ are the large-scale fading and radar cross-section (RCS) coefficient for the l-th ST, respectively. $\boldsymbol{a}_N(\theta_l) = [1, \mathrm{e}^{\mathrm{j}\pi\sin(\theta_l)}, \ldots, \mathrm{e}^{\mathrm{j}\pi(N-1)\sin(\theta_l)}]^{\mathrm{T}}$ is

the array steering vector. $d_{t,l}$ and θ_l are the distance and angle of arrival (AoA) from the l-th ST to the BS, respectively.

On the other hand, the network topology is based on stochastic geometry and models associated distances to determine the large-scale fadings in the ISAC systems. Instead of assuming fixed locations of CUs and STs and deriving performance analyses under a specific network topology, the stochastic geometry introduces an additional source of randomness in the locations of ISAC systems. Specifically, the locations of CUs and STs are randomly generated and following the homogeneous Poisson point process (PPP) Φ_U and Φ_T with the density of λ_U and λ_T, respectively. Given the limited time-frequency resources, serving CUs and STs are confined to finite-sized geographic area $\mathcal{S}_U$ and $\mathcal{S}_T$. For ease of presentation, we sort the CUs and STs by their ascending distance from the BS and let $d_{U,k}$ and $d_{T,l}$ denote the distance of the k-th nearest CU and the l-th nearest ST from the BS, respectively. As such, the finite ISAC service areas can be expressed as $\mathcal{S}_U = \{(r,\theta) : r \in (0, d_{u,K}]\}$ and $\mathcal{S}_T = \{(r,\theta) : r \in (0, d_{t,L}]\}$. Specifically, the probability density function (PDF) of $d_{\chi,i}$ for $\chi \in \{U,T\}$ can be referenced from [19] and expressed as

$$f_{d_{\chi,i}}(r) = \mathrm{e}^{-\lambda_\chi \pi r^2} \frac{2(\lambda_\chi \pi r^2)^i}{r(i-1)!}. \tag{1}$$

Then, the average distance $\bar{d}_{\chi,i} = \mathbb{E}[d_{\chi,i}]$ can be given by $\bar{d}_{\chi,i} = \int_0^\infty r\mathrm{e}^{-\lambda_\chi \pi r^2} \frac{2(\lambda_\chi \pi r^2)^i}{r(i-1)!}\mathrm{d}r = \frac{\Gamma(i+\frac{1}{2})}{\sqrt{\lambda_\chi \pi}(i-1)!}$, where $\Gamma(x) = \int_0^\infty t^{x-1}\mathrm{e}^{-t}\mathrm{d}t$ is the gamma function.

3 Uplink ISAC process

At this stage, CUs transmit uplink pilots to facilitate channel estimation, while the BS also transmits pilots towards the directions of θ_l for $l \in \{1,\ldots,L\}$ to implement target detection. In view of the limited number of orthogonal pilot sequences available, i.e., $T_u < K + L$, pilot reuse between C&S processes is necessary. Let $\sqrt{T_u}\boldsymbol{v}_{U,k}$ and $\sqrt{T_u}\boldsymbol{v}_{T,l}$ denote the pilot sequence assigned to the k-th CU and l-th ST, respectively, with $\|\boldsymbol{v}_{U,k}\|^2 = \|\boldsymbol{v}_{T,l}\|^2 = 1$. As such, we have

$$\boldsymbol{v}_{\chi,k}^{\mathrm{H}} \boldsymbol{v}_{\chi',k'} = \begin{cases} 1, & k' \in \mathcal{P}_k, \\ 0, & \text{otherwise}, \end{cases} \tag{2}$$

where $\mathcal{P}_k$ denotes the set of indices of STs that share the same pilot sequence of the k-th CU. Then, the received superimposed signal at the BS is given by $\boldsymbol{Y}_P = \sum_{k=1}^K \sqrt{P_{U,k}T_u}\boldsymbol{h}_k \boldsymbol{v}_{U,k}^{\mathrm{H}} + \sum_{l=1}^L \sqrt{P_{T,l}T_u}\boldsymbol{G}_l \boldsymbol{w}_l \boldsymbol{v}_{T,l}^{\mathrm{H}} + \boldsymbol{N}_P$, where $P_{U,k}$ and $P_{T,l}$ are the transmit power of the k-th CU and the power allocated for the l-th ST, respectively. $\boldsymbol{w}_l$ is the transmit beamforming of the BS towards the direction of θ_l, i.e., the maximum ratio combining $\boldsymbol{w}_l = \frac{\boldsymbol{a}_N(\theta_l)}{\sqrt{N}}$. $\boldsymbol{N}_P$ denotes the additive white Gaussian noise (AWGN) with each element following $\mathcal{CN}(0, N_0)$ and N_0 is the noise power. In order to derive tractable theoretical results, it is assumed that the number of CUs and that of STs are equal, i.e., $K = L$, and that the i-th nearest CU and the i-th nearest ST share the same pilot sequences. Theoretical results for other scenarios can also develop through similar derivations.

In this considered scenario, we first project $\boldsymbol{Y}_P$ onto $\boldsymbol{v}_k$ to realize the ISAC functions for the k-th group of CU and ST, such as

$$\boldsymbol{y}_{P,k} = \boldsymbol{Y}_P \boldsymbol{v}_k = \sqrt{P_{U,k}T_u}\boldsymbol{h}_k + \sqrt{P_{T,k}T_u}\boldsymbol{G}_k \boldsymbol{w}_k + \boldsymbol{n}_{P,k}, \tag{3}$$

where $\boldsymbol{n}_{P,k} \sim \mathcal{CN}(0, N_0 \boldsymbol{I}_N)$.

3.1 Performance derivation of uplink ISAC process

In this part, we derive the C&S performance region by investigating the channel estimation NMSE and successful detection probability. Following the minimum mean square error (MMSE) estimation technology [24], the estimate $\hat{h}_k$ of $\boldsymbol{h}_k$ can be expressed as $\hat{h}_k = \sqrt{\mu_k \kappa_{u,k}}\bar{h}_k + \frac{P_{U,k}T_u\mu_k}{P_{U,k}T_u\mu_k + P_{T,k}T_uN\beta_{t,k} + N_0}\left(\frac{\boldsymbol{y}_{P,k}}{\sqrt{P_{U,k}T_u}} - \sqrt{\mu_k \kappa_{u,k}}\bar{h}_k\right)$, and follows $\mathcal{CN}(\sqrt{\mu_k \kappa_{u,k}}\bar{h}_k, \phi_k \boldsymbol{I}_N)$ with $\phi_k = \frac{P_{U,k}T_u\mu_k^2}{P_{U,k}T_u\mu_k + P_{T,k}T_uN\beta_{t,k} + N_0}$.

Besides, the MMSE estimator also indicates that the estimation error $\boldsymbol{e}_k = \boldsymbol{h}_k - \hat{h}_k \sim \mathcal{CN}(\mathbf{0}, (\mu_k - \phi_k)\boldsymbol{I}_N)$ and is independent with $\hat{h}_k$. Hence, the NMSE of the k-th CU channel estimation can be expressed as

$$\varrho_k = \mathbb{E}\left\{\frac{\|\boldsymbol{e}_k\|^2}{\|\boldsymbol{h}_k\|^2}\right\} = \frac{\mu_k - \phi_k}{\mu_k}. \tag{4}$$

Then, the BS proceeds with the detection of the k-th ST. Let $\boldsymbol{r}_{P,k}$ denote the residual result as $\boldsymbol{y}_{P,k}$ minus the estimated communication part to solve the subsequent target detection problem. Specifically, the existence or absence of the k-th ST can be converted into a binary hypothesis, i.e., $\mathcal{H}_1$ and $\mathcal{H}_0$, as

$$\boldsymbol{r}_{P,k} = \begin{cases} \sqrt{P_{U,k}T_u}(\boldsymbol{h}_k - \hat{h}_k) + \boldsymbol{n}_{P,k}, & \text{under } \mathcal{H}_0, \\ \sqrt{P_{U,k}T_u}(\boldsymbol{h}_k - \hat{h}_k) + \sqrt{P_{T,k}T_u}\boldsymbol{G}_k\boldsymbol{w}_k + \boldsymbol{n}_{P,k}, & \text{under } \mathcal{H}_1. \end{cases} \tag{5}$$

The detection test can be further converted to a comparison between the predefined threshold ϵ_d and generalized likelihood ratio test (GLRT) [25] function as

$$\Lambda(\boldsymbol{r}_{P,k}) = \ln\frac{f(\boldsymbol{r}_{P,k}|\mathcal{H}_1)}{f(\boldsymbol{r}_{P,k}|\mathcal{H}_0)} = -\frac{\|\boldsymbol{r}_{P,k} - \sqrt{P_{T,k}T_uN\beta_{t,k}}\zeta_k\boldsymbol{a}_N(\theta_k)\|^2}{N_0 + P_{U,k}T_u(\mu_k - \phi_k)} + \frac{\|\boldsymbol{r}_{P,k}\|^2}{N_0 + P_{U,k}T_u(\mu_k - \phi_k)}, \tag{6}$$

where $f(\boldsymbol{r}_{P,k}|\mathcal{H}_1)$ and $f(\boldsymbol{r}_{P,k}|\mathcal{H}_0)$ are the likelihood functions under two hypothesis. Then, we obtain the unknown variable $\varpi_k = \sqrt{\beta_{t,k}}\zeta_k$ by maximum likelihood estimate, i.e.,

$$\widehat{\varpi_k} = \arg\max_{\varpi_k} f(\boldsymbol{r}_{P,k}|\mathcal{H}_1) = \arg\min_{\varpi_k} \|\boldsymbol{r}_{P,k} - \sqrt{P_{T,k}T_uN\beta_{t,k}}\zeta_k\boldsymbol{a}_N(\theta_k)\|^2 = \frac{\boldsymbol{a}_N^{\mathrm{H}}(\theta_k)\boldsymbol{r}_{P,k}}{\sqrt{P_{U,k}T_uN}N}. \tag{7}$$

Taking the estimate $\widehat{\varpi_k}$ into the GLRT function, it reduces to

$$\Lambda(\boldsymbol{r}_{P,k}) = \frac{\|\boldsymbol{r}_{P,k}\|^2 - \|\boldsymbol{r}_{P,k} - \frac{1}{N}\boldsymbol{a}_N(\theta_k)\boldsymbol{a}_N^{\mathrm{H}}(\theta_k)\boldsymbol{r}_{P,k}|^2}{N_0 + P_{U,k}T_u(\mu_k - \phi_k)} = \frac{\|\boldsymbol{r}_{P,k}^{\mathrm{H}}\boldsymbol{a}_N(\theta_k)\|^2}{N[N_0 + P_{U,k}T_u(\mu_k - \phi_k)]}.$$

The successful detection probability of the k-th ST is given by $P_{D,k} = \mathbb{P}(\Lambda(\boldsymbol{r}_{P,k}) > \epsilon_d \,|\mathcal{H}_1)$. Under the hypothesis $\mathcal{H}_1$, the variable follows $\boldsymbol{r}_{P,k}^{\mathrm{H}}\boldsymbol{a}_N(\theta_k) \sim \mathcal{CN}(\sqrt{P_{T,k}T_uN\beta_{t,k}}\zeta_k^*N, [N_0 + P_{U,k}T_u(\mu_k - \phi_k)]N)$. Thus, we have $|\frac{\sqrt{2}\boldsymbol{r}_{P,k}^{\mathrm{H}}\boldsymbol{a}_N(\theta_k)}{\sqrt{[N_0+P_{U,k}T_u(\mu_k-\phi_k)]N}}|^2 \sim \chi_2^2(\frac{2P_{T,k}T_uN^2\beta_{t,k}|\zeta_k|^2}{N_0+P_{U,k}T_u(\mu_k-\phi_k)})$. We can finally obtain the probability of successful detection as

$$P_{D,k} = \mathbb{P}\left(\frac{2\|\boldsymbol{r}_{P,k}^{\mathrm{H}}\boldsymbol{a}_N(\theta_k)\|^2}{N[N_0 + P_{U,k}T_u(\mu_k - \phi_k)]} > 2\epsilon_d \Big| \mathcal{H}_1\right) = Q_1\left(\sqrt{\frac{2P_{T,k}T_uN^2\beta_{t,k}|\zeta_k|^2}{N_0 + P_{U,k}T_u(\mu_k - \phi_k)}}, \sqrt{2\epsilon_d}\right), \tag{8}$$

where $Q_1(\cdot,\cdot)$ is the Marcum Q-function of order 1.

3.2 Joint coverage analysis of uplink ISAC performance

Regarding the performance analysis in the uplink ISAC process, we focus on the accuracy of the channel estimation for the CUs and the successful detection probability for the STs. Then, the joint coverage of uplink C&S performance for the K-th group CU and ST is investigated with $\|\zeta_K\|^2 = 1$, such as

$$P_{u,\mathrm{cov}}^{CS}(\epsilon_u^C, \epsilon_u^S) = \mathbb{P}\left\{\varrho_K \leqslant \epsilon_u^C, P_{D,K} \geqslant \epsilon_u^S\right\}, \tag{9}$$

which defines the joint probability that the channel estimation NMSE is not larger than the threshold ϵ_u^C and the successful detection probability is not smaller than the threshold ϵ_u^S simultaneously. In order to develop more critical theoretical results, the minor effects of N_0 can be neglected in the subsequent performance evaluation. We first study the coverage behaviors of the C&S processes separately, and have

$$P_{u,\mathrm{cov}}^{C}(\epsilon_u^C) = \mathbb{P}\left\{\frac{\mu_K - \phi_K}{\mu_K} \leqslant \epsilon_u^C\right\} = \mathbb{P}\left\{\frac{\mu_K}{\beta_{t,K}} \geqslant \frac{(1-\epsilon_u^C)P_{T,K}N}{\epsilon_u^C P_{U,K}}\right\}. \tag{10}$$

As for the coverage performance of the sensing function, it is not tractable to deal with the Marcum Q-function due to its non-closed formulation. Notice that $Q_1(a,b)$ is an increasing function with respect to a. Hence, the sensing coverage probability can be converted into

$$P_{u,\mathrm{cov}}^{S}(\epsilon_u^S)=\mathbb{P}\left\{\frac{2P_{T,K}T_uN^2\beta_{t,K}}{P_{U,K}T_u(\mu_K-\phi_K)}\geqslant\bar{\epsilon}_u^S\right\}=\begin{cases}\mathbb{P}\left\{\frac{\mu_K}{\beta_{t,K}}\leqslant\frac{2P_{T,K}N^2}{\bar{\epsilon}_u^SP_{U,K}-2P_{U,K}N}\right\}, & \bar{\epsilon}_u^S>2N,\\ 1, & \bar{\epsilon}_u^S\leqslant 2N,\end{cases}\tag{11}$$

where $\bar{\epsilon}_u^S$ can be obtained from $\epsilon_u^S=Q_1(\sqrt{\bar{\epsilon}_u^S},\sqrt{2\epsilon_d})$.

Remark 1. The condition for the probability of 1 in (11) indicates that the successful detection probability achieves at least $Q_1(\sqrt{2N},\sqrt{2\epsilon_d})$ thanks to the spatial beamforming gain for the sensing function.

Combining the coverage analyses of the separate functions in (10) and (11), we derive the joint coverage probability as

$$P_{u,\mathrm{cov}}^{CS}(\epsilon_u^C,\epsilon_u^S)=\begin{cases}\mathbb{P}\left\{\frac{(1-\epsilon_u^C)P_{T,K}N}{\epsilon_u^CP_{U,K}}\leqslant\frac{\mu_K}{\beta_{t,K}}\leqslant\frac{2P_{T,K}N^2}{\bar{\epsilon}_u^SP_{U,K}-2P_{U,K}N}\right\}, & \bar{\epsilon}_u^S>2N \text{ and } \epsilon_u^C\geqslant 1-\frac{2N}{\bar{\epsilon}_u^S},\\ \mathbb{P}\left\{\frac{\mu_K}{\beta_{t,K}}\geqslant\frac{(1-\epsilon_u^C)P_{T,K}N}{\epsilon_u^CP_{U,K}}\right\}, & \bar{\epsilon}_u^S\leqslant 2N \text{ and } \epsilon_u^C\geqslant 1-\frac{2N}{\bar{\epsilon}_u^S},\\ 0, & \epsilon_u^C<1-\frac{2N}{\bar{\epsilon}_u^S}.\end{cases}\tag{12}$$

Remark 2. Based on the upper and lower bounds on the integral in (12), a linear scaling law between $P_{U,K}$ and $P_{T,K}$ is established. This implies that when the transmit power of the CU and the power allocated to the ST increase at the same rate, the coverage probabilities for communication, sensing, and ISAC remain constant. Furthermore, a linear scaling law between λ_U and λ_T^2 is observed, as expressed by $\frac{\mu_K}{\beta_{t,K}}\leftrightarrow\frac{d_{U,K}^{-\alpha}}{d_{T,K}^{-2\alpha}}$ and $\frac{d_{U,K}^{-\alpha}}{d_{T,K}^{-2\alpha}}\leftrightarrow(\frac{\lambda_U}{\lambda_T^2})^{\frac{\alpha}{2}}$ from the derivation of (1), where $a\leftrightarrow b$ means the linear relationship between a and b.

Theorem 1. The joint coverage probability of the uplink ISAC process is given by

$$P_{u,\mathrm{cov}}^{CS}(\epsilon_u^C,\epsilon_u^S)=\begin{cases}F_Z\left(\left(\frac{\epsilon_u^CP_{U,K}}{(1-\epsilon_u^C)P_{T,K}N(1+\kappa_{u,K})}\right)^{\frac{1}{\alpha}}\right)-F_Z\left(\left(\frac{(\bar{\epsilon}_u^S-2N)P_{U,K}}{2P_{T,K}N^2(1+\kappa_{u,K})}\right)^{\frac{1}{\alpha}}\right), & \bar{\epsilon}_u^S>2N \text{ and } \epsilon_u^C\geqslant 1-\frac{2N}{\bar{\epsilon}_u^S},\\ F_Z\left(\left(\frac{\epsilon_u^CP_{U,K}}{(1-\epsilon_u^C)P_{T,K}N(1+\kappa_{u,K})}\right)^{\frac{1}{\alpha}}\right), & \bar{\epsilon}_u^S\leqslant 2N \text{ and } \epsilon_u^C\geqslant 1-\frac{2N}{\bar{\epsilon}_u^S},\\ 0, & \epsilon_u^C<1-\frac{2N}{\bar{\epsilon}_u^S},\end{cases}\tag{13}$$

where $F_Z(t)=\int_0^t f_Z(z)\mathrm{d}z$ is the cumulative distribution function (CDF) of $\frac{d_{U,K}}{d_{T,K}^2}$, $f_Z(z)$ is given by $f_Z(z)=\frac{2^{-3K+1}(\lambda_U\pi z^2)^{-\frac{K}{2}}(3K-1)!(\lambda_T\pi)^K}{z((K-1)!)^2}\mathcal{U}(\frac{3K}{2},\frac{1}{2},\frac{\lambda_T^2\pi}{4\lambda_Uz^2})$ and $\mathcal{U}(a,b,c)$ is the confluent hypergeometric function with $\mathcal{U}(a,b,c)=\frac{1}{\Gamma(a)}\int_0^\infty \mathrm{e}^{-ct}t^{a-1}(1+t)^{b-a-1}\mathrm{d}t$. The derivation process can refer to Appendix A.

The impact of key system parameters on the coverage probability reveals the fundamental trade-offs among the power allocation and distribution density of the CUs and STs for ISAC performance. Specifically, increasing $P_{U,K}$ enhances the communication performance, but weakens the sensing performance, thereby affecting the associated coverage probability. The increase in $P_{T,K}$ has the opposite trend. In a similar way, increasing λ_U and λ_T respectively improves the C&S coverage, as well as undermines the S&C coverage, for $\mu_K\leftrightarrow\lambda_U^{\frac{\alpha}{2}}$ and $\beta_{t,K}\leftrightarrow\lambda_T^{\alpha}$. The condition for the probability of 0 in Theorem 1 also provides profound insights into the coupling effects as the following corollary.

Corollary 1. When the probability of successful detection reaches $Q_1(\sqrt{\bar{\epsilon}_u^S},\sqrt{2\epsilon_d})$, the NMSE of channel estimation cannot be lower than $1-\frac{2N}{\bar{\epsilon}_u^S}$.

The fundamental limits of C&S performance are due to the channel coupling effects in ISAC systems. While improved channel estimation can mitigate the noise effect of the detection problem in (5), its decreased NMSE also implies that the power of the communication part $P_{U,K}\mu_K^2$ becomes stronger than that of the sensing part $P_{T,K}N\beta_{t,K}$, as shown in (4). This imbalance can ultimately constrain the successful detection probability in turn.

4 Downlink ISAC process

During the downlink process, the BS transmits superimposed signals to simultaneously transmit data to users and sense target parameters through echoes. To relieve the signal processing challenges, it is assumed that the downlink transmission is divided into L intervals, with the l-th ST being sensed in the l-th interval. Specifically, the transmitted signal in the l-th interval is written as $\boldsymbol{X}_{d,l} = \sqrt{P_{d,l}\rho}\sum_{k=1}^{K}\boldsymbol{w}_{U,k}\boldsymbol{s}_{U,k} + \sqrt{P_{d,l}(1-\rho)}\boldsymbol{w}_{T,l}\boldsymbol{s}_{T,l}$, where $P_{d,l}$ is the transmit power of the BS at the l-th interval, and $\rho \in [0,1]$ is the allocation factor for the communication function. $\boldsymbol{w}_{U,k} \in \mathbb{C}^{N\times 1}$ and $\boldsymbol{w}_{T,l} \in \mathbb{C}^{N\times 1}$ are the beamforming vectors for the k-th CU and l-th ST, respectively, satisfying $\mathbb{E}\{\|\boldsymbol{w}_{U,k}\|^2\} \leqslant 1$ and $\mathbb{E}\{\|\boldsymbol{w}_{T,l}\|^2\} \leqslant 1$. $\boldsymbol{s}_{U,k} \in \mathbb{C}^{1\times T_d}$ and $\boldsymbol{s}_{T,l} \in \mathbb{C}^{1\times T_d}$ are the transmitted symbols to the k-th CU and l-th ST, respectively and orthogonal to each other. Then, the received signal of the k-th CU is expressed as

$$\boldsymbol{y}_{U,k} = \sqrt{P_{d,l}\rho}\sum_{k=1}^{K}\boldsymbol{h}_k^{\mathrm{H}}\boldsymbol{w}_{U,k}\boldsymbol{s}_{U,k} + \sqrt{P_{d,l}(1-\rho)}\boldsymbol{h}_k^{\mathrm{H}}\boldsymbol{w}_{T,l}\boldsymbol{s}_{T,l} + \boldsymbol{n}_{d,k}, \tag{14}$$

where $\boldsymbol{n}_{d,k}$ is the AWGN at the k-th CU. Since the users are not aware of the instantaneous channel state information (CSI), the k-th CU treats the statistical CSI of $\mathbb{E}\{\boldsymbol{h}_k^{\mathrm{H}}\boldsymbol{w}_{U,k}\}$ as the desired signal and the corresponding signal to interference plus noise ratio (SINR) [26] can be expressed as

$$\gamma_k = \frac{P_{d,l}\rho\|\mathbb{E}\{\boldsymbol{h}_k^{\mathrm{H}}\boldsymbol{w}_{U,k}\}\|^2}{P_{d,l}\rho\sum_{i=1}^{K}\mathbb{E}\left\{\|\boldsymbol{h}_k^{\mathrm{H}}\boldsymbol{w}_{U,i}\|^2\right\} - P_{d,l}\rho\|\mathbb{E}\{\boldsymbol{h}_k^{\mathrm{H}}\boldsymbol{w}_{U,k}\}\|^2 + P_{d,l}(1-\rho)\mathbb{E}\left\{\|\boldsymbol{h}_k^{\mathrm{H}}\boldsymbol{w}_{T,l}\|^2\right\} + N_0}. \tag{15}$$

On the other hand, the BS utilizes the echo signals to sense the target parameters, i.e., the direction of AoA θ_l. The received signal at the BS is given by

$$\boldsymbol{Y}_{B,l} = \boldsymbol{G}_l\boldsymbol{X}_{d,l} + \boldsymbol{N}_{B,l} = \sqrt{\beta_{t,l}}\zeta_l\boldsymbol{a}_N(\theta_l)\boldsymbol{a}_N^{\mathrm{H}}(\theta_l)\boldsymbol{X}_{d,l} + \boldsymbol{N}_{B,l}, \tag{16}$$

where $\boldsymbol{N}_{B,l}$ is the AWGN at the BS. Vectorize both sides of the equation and obtain

$$\boldsymbol{y}_{B,l} = \sqrt{\beta_{t,l}}\zeta_l\mathrm{vec}\left(\boldsymbol{a}_N(\theta_l)\boldsymbol{a}_N^{\mathrm{H}}(\theta_l)\boldsymbol{X}_{d,l}\right) + \boldsymbol{n}_{B,l}, \tag{17}$$

where $\boldsymbol{n}_{B,l} = \mathrm{vec}(\boldsymbol{N}_{B,l})$. The unknown parameter vector is written as $\boldsymbol{\xi}_l = [\theta_l, \mathrm{Re}(\varpi), \mathrm{Im}(\varpi)]^{\mathrm{T}}$ and the noiseless signal is $\boldsymbol{u}_{B,l} = \varpi_l\mathrm{vec}\left(\boldsymbol{a}_N(\theta_l)\boldsymbol{a}_N^{\mathrm{H}}(\theta_l)\boldsymbol{X}_{d,l}\right)$. Then, the estimation performance can be evaluated by the CRLB as $C_l(\theta_l) = [(\boldsymbol{F}_l)^{-1}]_{1,1}$, where the FIM can be written as in [24]

$$[\boldsymbol{F}_l]_{\xi_i,\xi_j} = \frac{2}{N_0}\mathrm{Re}\left\{\frac{\partial\boldsymbol{u}_{B,l}^{\mathrm{H}}}{\partial\xi_i}\frac{\partial\boldsymbol{u}_{B,l}}{\partial\xi_j}\right\}. \tag{18}$$

We have $[\boldsymbol{F}_l]_{\theta_l,\theta_l} = \frac{2|\varpi|^2}{N_0}\mathrm{tr}(\breve{\boldsymbol{A}}(\theta_l)\boldsymbol{X}_{d,l}\boldsymbol{X}_{d,l}^{\mathrm{H}}\breve{\boldsymbol{A}}^{\mathrm{H}}(\theta_l))$, $[\boldsymbol{F}_l]_{\theta_l,\boldsymbol{\varpi}} = \frac{2}{N_0}\mathrm{Re}\{\varpi^*\mathrm{tr}(\boldsymbol{A}(\theta_l)\boldsymbol{X}_{d,l}\boldsymbol{X}_{d,l}^{\mathrm{H}}\breve{\boldsymbol{A}}^{\mathrm{H}}(\theta_l))\}$, and $[\boldsymbol{F}_l]_{\boldsymbol{\varpi},\boldsymbol{\varpi}} = \frac{2}{N_0}\mathrm{tr}(\boldsymbol{A}(\theta_l)\boldsymbol{X}_{d,l}\boldsymbol{X}_{d,l}^{\mathrm{H}}\boldsymbol{A}^{\mathrm{H}}(\theta_l))\boldsymbol{I}$, which are based on $\frac{\partial\mathrm{vec}(f(x))}{\partial x} = \mathrm{vec}(\frac{\partial f(x)}{\partial x})$ and $\mathrm{vec}^{\mathrm{H}}(\boldsymbol{A})\mathrm{vec}(\boldsymbol{B}) = \mathrm{tr}(\boldsymbol{A}^{\mathrm{H}}\boldsymbol{B})$, and let $\boldsymbol{A}(\theta_l) = \boldsymbol{a}_N(\theta_l)\boldsymbol{a}_N^{\mathrm{H}}(\theta_l)$, $\breve{\boldsymbol{A}}(\theta_l) = \breve{a}_N(\theta_l)\boldsymbol{a}_N^{\mathrm{H}}(\theta_l) + \boldsymbol{a}_N(\theta_l)\breve{a}_N^{\mathrm{H}}(\theta_l)$, and $\breve{a}_N(\theta_l) = [0, \mathrm{j}\pi\cos(\theta_l)\mathrm{e}^{\mathrm{j}\pi\sin(\theta_l)}, \ldots, \mathrm{j}\pi(N-1)\cos(\theta_l)\mathrm{e}^{\mathrm{j}\pi(N-1)\sin(\theta_l)}]^{\mathrm{T}}$. Then, the MSE of θ_l is lower bounded by $C_l(\theta_l)$ as

$$\begin{aligned}\left[\boldsymbol{F}_l^{-1}\right]_{1,1} &= \left[[\boldsymbol{F}_l]_{\theta_l,\theta_l} - [\boldsymbol{F}_l]_{\theta_l,\boldsymbol{\varpi}}[\boldsymbol{F}_l]_{\boldsymbol{\varpi},\boldsymbol{\varpi}}^{-1}[\boldsymbol{F}_l]_{\theta_l,\boldsymbol{\varpi}}^{\mathrm{T}}\right]_{1,1}^{-1} \\ &= \frac{N_0}{2|\varpi_l|^2[\mathrm{tr}(\breve{\boldsymbol{A}}(\theta_l)\boldsymbol{X}_{d,l}\boldsymbol{X}_{d,l}^{\mathrm{H}}\breve{\boldsymbol{A}}^{\mathrm{H}}(\theta_l)) - \frac{|\mathrm{tr}(\boldsymbol{A}(\theta_l)\boldsymbol{X}_{d,l}\boldsymbol{X}_{d,l}^{\mathrm{H}}\breve{\boldsymbol{A}}^{\mathrm{H}}(\theta_l))|^2}{\mathrm{tr}(\boldsymbol{A}(\theta_l)\boldsymbol{X}_{d,l}\boldsymbol{X}_{d,l}^{\mathrm{H}}\boldsymbol{A}^{\mathrm{H}}(\theta_l))}]}.\end{aligned} \tag{19}$$

4.1 Performance derivation of downlink ISAC process

In this part, we derive the C&S performance region by investigating the communication sum-rate and sensing sum-root-CRLB. We select maximum ratio transmission precoding for ISAC functions due to its low computational complexity and remarkable performance, which are given by $\boldsymbol{w}_{U,k} = \frac{\hat{\boldsymbol{h}}_k}{\sqrt{\mathbb{E}\{\|\hat{\boldsymbol{h}}_k\|^2\}}}$ and $\boldsymbol{w}_{T,l} = \frac{\boldsymbol{a}_N(\theta_l)}{\sqrt{N}}$.

Based on the developed precoding vectors, the SINR is given in the following lemma.

Lemma 1. The SINR of the k-th CU in ISAC systems can be expressed as

$$\gamma_k = \frac{\rho(\mu_k\kappa_{u,k}\|\bar{h}_k\|^2 + \phi_k N)}{\Sigma_{\text{Comm}} + (1-\rho)(\mu_k\kappa_{u,k}\|\boldsymbol{a}_N^{\text{H}}(\theta_l)\bar{h}_k\|^2 + \mu_k N)/N + \frac{N_0}{P_{d,l}}}, \tag{20}$$

where $\Sigma_{\text{Comm}} = \rho\sum_{i=1}^{K}\frac{\mu_i\mu_k\kappa_{u,i}\kappa_{u,k}\|\bar{h}_k^{\text{H}}\bar{h}_i\|^2+\mu_i\mu_k\kappa_{u,i}\|\bar{h}_i\|^2+\phi_i\mu_k\kappa_{u,k}\|\bar{h}_k\|^2+\phi_i\mu_k N}{\mu_i\kappa_{u,i}\|\bar{h}_i\|^2+\phi_i N} - \frac{\mu_k^2\kappa_{u,k}^2\|\bar{h}_k\|^4}{\mu_k\kappa_{u,k}\|\bar{h}_k\|^2+\phi_k N}$ is the sum of multi-CU interference as well as the loss of using the statistical CSI.

Proof. Please refer to Appendix B.

The SINR expression can be further simplified when the LoS paths of CUs are all deterministic as single paths, i.e., $\bar{h}_k = \boldsymbol{a}_N(\varphi_k)$, where φ_k is the AoA from the k-th CU to the BS. In this case, there exists $\frac{1}{N}\boldsymbol{a}_N^{\text{H}}(\varphi_k)\boldsymbol{a}_N(\varphi_i) \overset{N\to\infty}{\longrightarrow} 0$, for any $\varphi_k \neq \varphi_i$.

Lemma 2. When the number of BS antennas tends to infinity, the SINR of the k-th CU in the ISAC systems can be further simplified as

$$\bar{\gamma}_k = \frac{\rho N\left(\mu_k\kappa_{u,k} + \phi_k\right)}{\rho\sum_{i=1}^{K}\left(\mu_i\mu_k\kappa_{u,i} + \phi_i\mu_k\kappa_{u,k} + \phi_i\mu_k\right)/\left(\mu_i\kappa_{u,i} + \phi_i\right) + (1-\rho)\mu_k + \frac{N_0}{P_{d,l}}}. \tag{21}$$

As for the CRLB derivation of the sensing process, the theoretical results are given as follows.

Lemma 3. The CRLB of the direction of the l-th ST is written as

$$C_l(\theta_l) = \frac{N_0\Pi_{AA}^l}{2|\varpi_l|^2 P_{d,l}T_d[\Pi_{\breve{A}\breve{A}}^l\Pi_{AA}^l - \Pi_{A\breve{A}}^{l,\text{square}}]}, \tag{22}$$

where

$$\Pi_{AA}^l = \rho\sum_{k=1}^{K}\sum_{i=1}^{K}\frac{\mu_k\mu_i\kappa_{u,k}\kappa_{u,i}\text{tr}\left(\boldsymbol{a}_N^{\text{H}}(\theta_l)\bar{h}_k\bar{h}_i^{\text{H}}\boldsymbol{a}_N(\theta_l)\right)}{\sqrt{\left(\mu_k\kappa_{u,k}+\phi_k\right)\left(\mu_i\kappa_{u,i}+\phi_i\right)}} + \rho\sum_{k=1}^{K}\frac{\phi_k N^2}{\mu_k\kappa_{u,k}+\phi_k} + (1-\rho)N^2,$$

$$\begin{aligned}\Pi_{\breve{A}\breve{A}}^l = \rho\sum_{k=1}^{K}\sum_{i=1}^{K}&\sqrt{\frac{\mu_k\mu_i\kappa_{u,k}\kappa_{u,i}}{\left(\mu_k\kappa_{u,k}+\phi_k\right)\left(\mu_i\kappa_{u,i}+\phi_i\right)}}\Bigg[\frac{N-1}{2}\text{j}\pi\cos(\theta_l)\text{tr}\left(\boldsymbol{a}_N^{\text{H}}(\theta_l)\bar{h}_k\bar{h}_i^{\text{H}}\breve{a}_N(\theta_l)\right)\\
&+\frac{(N-1)(2N-1)}{6}\pi^2\cos^2(\theta_l)\text{tr}(\boldsymbol{a}_N^{\text{H}}(\theta_l)\bar{h}_k\bar{h}_i^{\text{H}}\cdot\boldsymbol{a}_N(\theta_l)) + \text{tr}\left(\breve{a}_N^{\text{H}}(\theta_l)\bar{h}_k\bar{h}_i^{\text{H}}\breve{a}_N(\theta_l)\right)\\
&-\frac{N-1}{2}\text{j}\pi\cos(\theta_l)\text{tr}(\breve{a}_N^{\text{H}}(\theta_l)\bar{h}_k\bar{h}_i^{\text{H}}\boldsymbol{a}_N(\theta_l))\Bigg] + \rho\frac{N(N^2-1)}{6}\pi^2\cos^2(\theta_l)\cdot\sum_{k=1}^{K}\frac{\phi_k}{\mu_k\kappa_{u,k}+\phi_k}\\
&+(1-\rho)\frac{N^2(N^2-1)}{12}\pi^2\cos^2(\theta_l),\end{aligned}$$

and

$$\Pi_{A\breve{A}}^{l,\text{square}} = \rho^2\left|\sum_{k=1}^{K}\sum_{i=1}^{K}\frac{\sqrt{\mu_k\mu_i\kappa_{u,k}\kappa_{u,i}}\left(\text{tr}(\boldsymbol{a}_N^{\text{H}}(\theta_l)\bar{h}_k\bar{h}_i^{\text{H}}\breve{a}_N(\theta_l)) - \frac{N-1}{2}\text{j}\pi\cos(\theta_l)\text{tr}(\boldsymbol{a}_N^{\text{H}}(\theta_l)\bar{h}_k\bar{h}_i^{\text{H}}\boldsymbol{a}_N(\theta_l))\right)}{\sqrt{\left(\mu_k\kappa_{u,k}+\phi_k\right)\left(\mu_i\kappa_{u,i}+\phi_i\right)}}\right|^2.$$

Proof. Please refer to Appendix C.

The CRLB expression in (22) can also be simplified in some special cases. Thus, we investigate the scenario when the direction angles of the CUs and STs differ by more than $2/N$, which is easily satisfied for infinite antennas.

Lemma 4. When the number of BS antennas tends to infinity, the CRLB of the l-th ST in ISAC systems can be expressed as

$$\bar{C}_l(\theta_l) = \frac{6N_0}{|\varpi_l|^2 P_{d,l}(1-\rho)T_d N^2(N^2-1)\pi^2\cos^2(\theta_l)}. \tag{23}$$

Proof. Please refer to Appendix D.

Fundamental trade-offs can be revealed through the C&S performance region between the communication SINR in (21) and sensing CRLB in (23). We further investigate their mutual effects, such as the ratio of the interference power caused by the sensing function against communication performance for the k-th CU in (21) and the ratio of enhancement power brought by the communication function to sensing performance for the k-th ST in (22), defined as

$$\Psi_k = \frac{\rho N\left(\mu_k\kappa_{u,k}+\phi_k\right)}{(1-\rho)\mu_k} = \frac{\rho}{1-\rho}N\left(\kappa_{u,k}+\frac{P_{U,k}\mu_k}{P_{U,k}\mu_k+P_{T,k}N\beta_{t,k}+N_0}\right), \tag{24}$$

and

$$\Omega_k = \frac{\frac{1}{12}P_{d,k}(1-\rho)N^2(N^2-1)\pi^2\cos^2(\theta_k)}{\frac{1}{6}P_{d,k}\rho N(N^2-1)\pi^2\cos^2(\theta_k)\frac{\phi_k}{\mu_k\kappa_{u,k}+\phi_k}} = \frac{(1-\rho)N}{2\rho}\left(\kappa_{u,K}+1+\frac{\kappa_{u,K}(P_{T,k}N\beta_{t,k}+N_0)}{P_{U,k}\mu_k}\right). \tag{25}$$

Remark 3. When $\kappa_{u,k}\to\infty$, i.e., in the LoS-dominated ISAC systems, the ratio factors become $\Psi_k\to\infty$ and $\Omega_k\to\infty$, which means that ISAC mutual interference $1/\Psi_k$ and mutual benefit $1/\Omega_k$ reduce to 0. On the other hand when the uplink channel estimation error is not considered, there can be $\frac{1-\rho}{\rho}\frac{1}{N(1+\kappa_{u,k})}$ interference power for the communication function, while $2\frac{\rho}{1-\rho}\frac{1}{N(1+\kappa_{u,k})}$ enhancement power for the sensing function.

Lemma 5. The ergodic sensing interference ratio and communication enhancement ratio by considering all possible locations of CUs and STs are converged to closed-form expressions as

$$\begin{aligned}\bar{\Omega}_k = \mathbb{E}\{\Omega_k\} =& \frac{(1-\rho)N}{2\rho}(\kappa_{u,k}+1)\\ &+\frac{(1-\rho)N}{2\rho}(\lambda_U\pi)^{-\frac{\alpha}{2}}\frac{\kappa_{u,k}(1+\kappa_{u,k})\Gamma(k+\frac{\alpha}{2})}{P_{U,k}\Gamma(k)}\left(\frac{N_0}{C_0}+(\lambda_T\pi)^{\alpha}P_{T,k}N\frac{\Gamma(k-\alpha)}{\Gamma(k)}\right),\end{aligned} \tag{26}$$

where $\Gamma(x)$ is the Gamma function and under $k>\alpha$, while

$$\begin{aligned}\bar{\Psi}_k = \mathbb{E}\{\Psi_k\} =& \frac{\rho N\kappa_{u,k}}{1-\rho}+\frac{\rho N}{(1-\rho)}\cdot\left(\frac{\lambda_U\pi P_{U,k}C_0}{(1+\kappa_{u,k})\left(P_TN\beta_{t,k}+N_0\right)}\right)^k E_k\left(\frac{\lambda_U\pi P_{U,k}C_0}{(1+\kappa_{u,k})\left(P_TN\beta_{t,k}+N_0\right)}\right)\\ &\cdot\exp\left(\frac{\lambda_U\pi P_{U,k}C_0}{(1+\kappa_{u,k})\left(P_TN\beta_{t,k}+N_0\right)}\right),\end{aligned} \tag{27}$$

where $E_k(x)=\int_1^{\infty}\mathrm{e}^{-xt}/t^k\mathrm{d}t$ is the exponential integral function and under the assumption $\alpha=2$.

Proof. Please refer to Appendix E.

4.2 Joint coverage analysis of downlink ISAC performance

Regarding the performance analysis in the downlink ISAC process, we focus on the maximum mutual interference and minimum mutual benefits assurance and give the joint coverage probability as

$$P_{d,\mathrm{cov}}^{CS}(\epsilon_d^C,\epsilon_d^S)=\mathbb{P}\left\{\frac{1}{\Psi_k}\leqslant\epsilon_d^C,\frac{1}{\Omega_k}\geqslant\epsilon_d^S\right\}, \tag{28}$$

which defines the joint coverage probability that the mutual interference is not larger than the threshold ϵ_d^C and the mutual benefit is not smaller than the threshold ϵ_d^S simultaneously. Similarly, we ignore the minor noise effect and further give the joint coverage probability as

$$\begin{aligned}P_{d,\mathrm{cov}}^{CS}(\epsilon_d^C,\epsilon_d^S) &= \mathbb{P}\left\{\frac{\rho}{1-\rho}N\left(\kappa_{u,k}+\frac{P_{U,k}\mu_k}{P_{U,k}\mu_k+P_{T,k}N\beta_{t,k}}\right)\geqslant\frac{1}{\epsilon_d^C},2\frac{\rho}{(1-\rho)N}\frac{\phi_k}{\mu_k\kappa_{u,k}+\phi_k}\geqslant\epsilon_d^S\right\}\\ &= \mathbb{P}\left\{\frac{P_{U,k}\mu_k}{P_{U,k}\mu_k+P_{T,k}N\beta_{t,k}}\geqslant\frac{1-\rho}{\rho\epsilon_d^CN}-\kappa_{u,k},\frac{\kappa_{u,k}P_{T,k}N\beta_{t,k}}{P_{U,k}\mu_k}\leqslant\frac{2\rho}{(1-\rho)N\epsilon_d^S}-\kappa_{u,k}-1\right\}.\end{aligned} \tag{29}$$

The following are categorized into three scenarios depending on the value of Rician factor $\kappa_{u,k}$. For large Rician factor, i.e. $\kappa_{u,k}>\frac{2\rho}{(1-\rho)N\epsilon_d^S}-1$, the joint coverage reduces to zero. For the case of $\frac{1-\rho}{\rho\epsilon_d^CN}\leqslant$

$\kappa_{u,k} \leqslant \frac{2\rho}{(1-\rho)N\epsilon_d^S} - 1$ when $\epsilon_d^S < \frac{2\rho^2\epsilon_d^C}{(1-\rho)(1-\rho+\rho\epsilon_d^C N)}$, the joint coverage probability reduces to $\mathbb{P}\{\frac{d_{U,k}}{d_{T,k}^2} \leqslant (\frac{P_{U,k}}{\kappa_{u,k}(1+\kappa_{u,k})P_{T,k}N}(\frac{2\rho}{(1-\rho)N\epsilon_d^S} - \kappa_{u,k} - 1))^{\frac{1}{\alpha}}\}$ and then to $F_Z((\frac{P_{U,k}}{\kappa_{u,k}(1+\kappa_{u,k})P_{T,k}N}(\frac{2\rho}{(1-\rho)N\epsilon_d^S} - \kappa_{u,k} - 1))^{\frac{1}{\alpha}})$.

The last case is for $\kappa_{u,k} < \min\{\frac{1-\rho}{\rho\epsilon_d^C N}, \frac{2\rho}{(1-\rho)\epsilon_d^S} - 1\}$, where the joint coverage is give by

$$\mathbb{P}\left\{\frac{d_{U,k}}{d_{T,k}^2} \leqslant \left(\frac{P_{U,k}}{P_{T,k}N(1+\kappa_{u,k})}\frac{\rho\epsilon_d^C N(1+\kappa_{u,k})+\rho-1}{1-\rho-\kappa_{u,k}\rho\epsilon_d^C N}\right)^{\frac{1}{\alpha}}, \right.$$
$$\left.\frac{d_{U,k}}{d_{T,k}^2} \leqslant \left(\frac{P_{U,k}}{\kappa_{u,k}(1+\kappa_{u,k})P_{T,k}N}\left(\frac{2\rho}{(1-\rho)N\epsilon_d^S} - \kappa_{u,k} - 1\right)\right)^{\frac{1}{\alpha}}\right\}$$

and written as

$$F_Z\left(\min\left\{\left(\frac{P_{U,k}}{P_{T,k}N(1+\kappa_{u,k})}\frac{\rho\epsilon_d^C N(1+\kappa_{u,k})+\rho-1}{1-\rho-\kappa_{u,k}\rho\epsilon_d^C N}\right)^{\frac{1}{\alpha}}, \right.\right.$$
$$\left.\left.\left(\frac{P_{U,k}}{\kappa_{u,k}(1+\kappa_{u,k})P_{T,k}N}\left(\frac{2\rho}{(1-\rho)N\epsilon_d^S} - \kappa_{u,k} - 1\right)\right)^{\frac{1}{\alpha}}\right\}\right).$$

Summarizing these scenarios yields

$$P_{d,\mathrm{cov}}^{CS}(\epsilon_d^C, \epsilon_d^S) =$$
$$\begin{cases} F_Z\left(\min\left\{\left(\frac{P_{U,k}(\rho\epsilon_d^C N(1+\kappa_{u,k})+\rho-1)}{P_{T,k}N(1+\kappa_{u,k})(1-\rho-\kappa_{u,k}\rho\epsilon_d^C N)}\right)^{\frac{1}{\alpha}}, \left(\frac{P_{U,k}(2\rho-(\kappa_{u,k}+1)(1-\rho)N\epsilon_d^S)}{\kappa_{u,k}(1+\kappa_{u,k})P_{T,k}N^2(1-\rho)\epsilon_d^S}\right)^{\frac{1}{\alpha}}\right\}\right), & \kappa_{u,k} < \min\left\{\frac{1-\rho}{\rho\epsilon_d^C N}, \frac{2\rho}{(1-\rho)N\epsilon_d^S} - 1\right\}, \\ F_Z\left(\left(\frac{P_{U,k}}{\kappa_{u,k}(1+\kappa_{u,k})P_{T,k}N}\left(\frac{2\rho}{(1-\rho)N\epsilon_d^S} - \kappa_{u,k} - 1\right)\right)^{\frac{1}{\alpha}}\right), & \epsilon_d^S < \frac{2\rho^2\epsilon_d^C}{(1-\rho)(1-\rho+\rho\epsilon_d^C N)} \text{and} \frac{1-\rho}{\rho\epsilon_d^C N} \leqslant \kappa_{u,k} \leqslant \frac{2\rho}{(1-\rho)N\epsilon_d^S} - 1, \\ 0, & \text{otherwise.} \end{cases} \tag{30}$$

The condition for the joint downlink ISAC probability of 0 provides profound insights into the coupling effects as the following corollary.

Corollary 2. The mutual interference cannot be below $\frac{1-\rho}{\rho N(1+\kappa_{u,k})}$, and the mutual benefit cannot be above $\frac{2\rho}{(1-\rho)N(1+\kappa_{u,k})}$.

For the first case regarding the communication coverage, when simultaneously satisfying $\frac{1-\rho}{\rho\epsilon_d^C N} - \kappa_{u,k} > 0$ and $\frac{P_{U,k}}{P_{T,k}N(1+\kappa_{u,k})}\frac{\rho\epsilon_d^C N(1+\kappa_{u,k})+\rho-1}{1-\rho-\kappa_{u,k}\rho\epsilon_d^C N} \leqslant 0$, the joint coverage reduces to zero. For the second case regarding the sensing coverage, when satisfying $\frac{2\rho}{(1-\rho)N\epsilon_d^S} - \kappa_{u,k} - 1 \leqslant 0$, the joint coverage reduces to zero. These cases mean that $\epsilon_d^C \leqslant \frac{1-\rho}{\rho N(1+\kappa_{u,k})}$ or $\epsilon_d^S \geqslant \frac{2\rho}{(1-\rho)N(1+\kappa_{u,k})}$ cannot occur, which are two ISAC analytical bounds to indicate fundamental limits of C&S performance.

Remark 4. It should be noted that there still exist channel coupling effects between uplink and downlink C&S performance when the ISAC network topology has not changed. In a similar way, we can derive that when the probability of uplink successful detection reaches $Q_1(\sqrt{\bar{\epsilon}_u^S}, \sqrt{2\epsilon_d})$, the downlink mutual interference cannot be below $\frac{\bar{\epsilon}_u^S(1-\rho)}{\rho N(2N+\kappa_{u,K}\bar{\epsilon}_u^S)}$ and the mutual benefit cannot be above $\frac{4\rho}{(1-\rho)(\bar{\epsilon}_u^S\kappa_{u,K}+2N)}$.

5 Numerical results

In this section, we present numerical results to demonstrate the fundamental trade-offs and coupling effects for uplink and downlink ISAC functions. These results can well validate the accuracy of our derived analytical expressions, including the successful detection probability and channel estimation NMSE for the uplink process, the sensing CRLB and communication rate for the downlink process, as well as their joint coverage probability. The results also illustrate the impact of various system parameters, such as the number of BS antennas, transmit power allocated to the communication/sensing function, the number of CUs/STs, and the Rician factor, on the C&S performance region and their joint coverage probability. The simulation further delves into several insights into scaling laws, asymptotic behaviors, and monotonicity

properties of ISAC systems. Additionally, they characterize analytical union bounds that establish the performance limits under coupling effects, offering a comprehensive understanding of the ISAC systems' practical capabilities.

5.1 Simulation settings

The densities of CUs and STs are $\lambda_U = 10^2$ km^{-2} and $\lambda_T = 10^3$ km^{-2}, respectively. The numbers of serving users and targets are $K = 4$ and $L = 4$, respectively. The BS is equipped with $N = 64$ antennas. The transmit power allocated to CUs and STs is $P_{U,k} = 0$ dB and $P_{T,l} = -10$ dB for $\forall k, l$, respectively. The path-loss coefficients are set as $C_0 = -30$ dB and $\alpha = 2.8$. The noise power of the ISAC process is $N_0 = -80$ dBm. Unless otherwise mentioned, other system parameters are listed as follows: $T_u = T_d = 64$, $\epsilon_d = 18$ dB, $\rho = 0.5$, $\kappa_{u,k} = 1$ for $\forall k$, $P_{d,l} = 0$ dB for $\forall l$.

5.2 Uplink ISAC performance

Figure 2 presents simulation results for the trade-off between the probability of missing detection $1-P_{D,K}$ and channel estimation NMSE ϱ_K, compared with Monte Carlo simulations under varying N and $P_{T,K}$. It demonstrates that the analytical results closely match the experimental outcomes, confirming the accuracy of our theoretical formulations. Furthermore, it can be observed that an increase in sensing power can decrease the probability of missing detection but also increase the channel estimation error. Additionally, increasing N significantly enhances the sensing detection performance, while strong sensing echo power adversely impairs channel estimation accuracy. In particular, when the number of BS antennas grows from 16 to 32, the probability of missing detection can be reduced by 62.5% at the cost of 2.88 dB increase in the channel estimation NMSE.

In Figure 3, we plot the coverage probability of C&S functions under different values of $[\lambda_U, \lambda_T, P_{U,K}, P_{T,K}]$. The results indicate that raising the density and transmit power of CUs significantly enhances the communication coverage probability but reduces the sensing coverage. Notably, it shows that these configurations all ensure the probability of successful detection exceeds $Q_1(\sqrt{2N}, \sqrt{2\epsilon_d})$ attributed to the spatial beamforming gain. Besides, the overlap between the first and third curves confirms the linear scaling laws between λ_U and λ_T^2, as well as between $P_{U,K}$ and $P_{T,K}$, which demonstrates that proportionally increasing the density and transmit power of CUs and STs yields the equivalent ISAC performance.

Figure 4 illustrates the monotonic behaviors of the coverage probabilities for C&S functions versus different numbers of BS antennas. An inverse trend is observed between C&S coverages, such as an increase in N or a decrease in K leading to reduced communication coverage but enhanced sensing coverage. This behavior is attributed to the spatial beamforming gain of order $\mathcal{O}(N)$ and squared path-loss attenuation term corresponding to the STs. Moreover, the effects of increasing N on C&S coverage probabilities are shown more pronounced at larger values of K.

Figure 5 depicts the joint ISAC coverage probability under various C&S thresholds. The Monte Carlo simulations are observed to well overlap the analytical surface, verifying the accuracy of Theorem 1. These results also provide critical insights into the inherent mutual effects between C&S performances. Specifically, the "ISAC analytical bound" surface consists of all points satisfying $\epsilon_u^C = 1 - \frac{2N}{\bar{\epsilon}_d^S}$ as derived in Corollary 1. The zero values within the ISAC bound in Figure 5 clearly indicate that the channel estimation NMSE cannot be lower than $1-\frac{2N}{\bar{\epsilon}_d^S}$. In particular, when the probability of successful detection increases from 58.4% to 98.1%, the minimum NMSE of channel estimation deteriorates from -18.13 to -5.64 dB in the ISAC systems.

5.3 Downlink ISAC performance

Subsequently, we examine the trade-off between uplink channel estimation NMSE and downlink communication throughput, and between uplink probability of missing detection and downlink root-CRLB for the K-th CU and ST in Figure 6. It can be observed that an increase in uplink pilot length generally improves the uplink C&S performance, but instead undermines the downlink C&S performance due to the reduced data length. However, there is a rise and then a decline in the communication throughput, which is due to an increase initially as the quality of uplink channel estimation improves, and later as the downlink data length decreases. Therefore, it is essential to determine the optimal pilot length to achieve a satisfactory trade-off between uplink and downlink C&S performance.

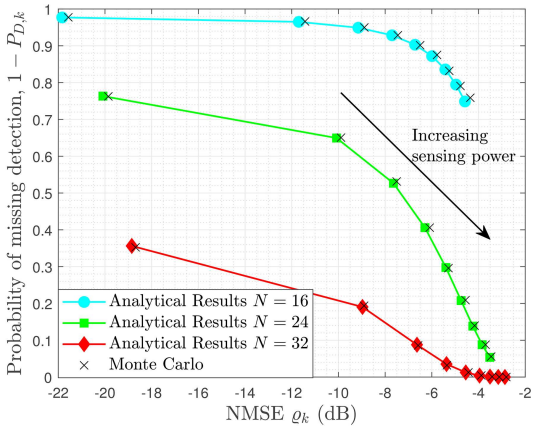

Figure 2 (Color online) Trade-offs between the probability of missing detection and channel estimation NMSE as $P_{T,K}$ increases from -20 to 0 dB with $d_{U,K} = 25$ m and $d_{T,K} = 10$ m.

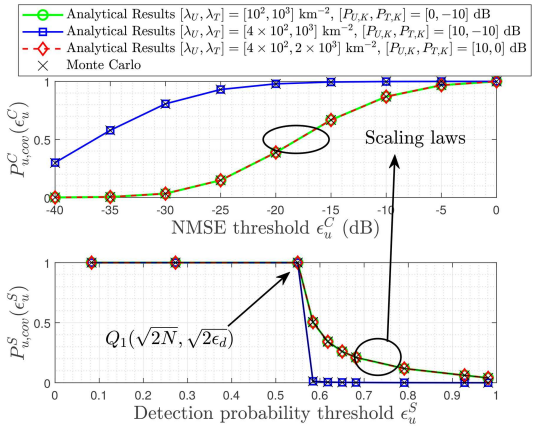

Figure 3 (Color online) Coverage probability of communication and sensing functions versus different density and transmit power of CUs and STs.

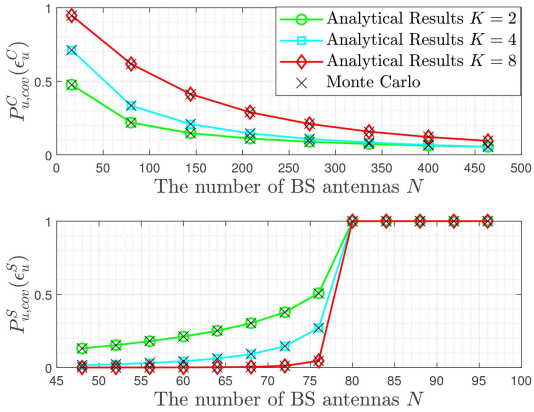

Figure 4 (Color online) Coverage probability of communication and sensing functions versus different N and K with $\epsilon_u^C = -20$ dB and $\epsilon_u^S = 0.9275$.

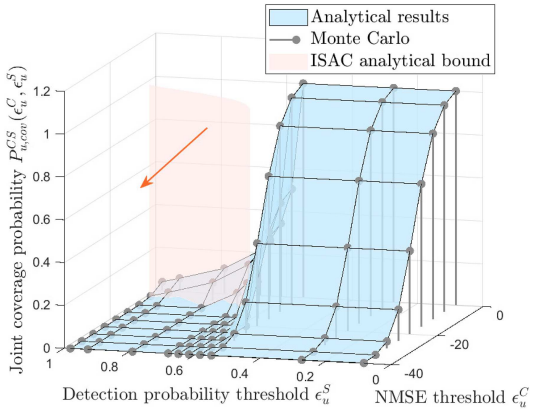

Figure 5 (Color online) Joint coverage probability of uplink ISAC performance versus different communication and sensing thresholds.

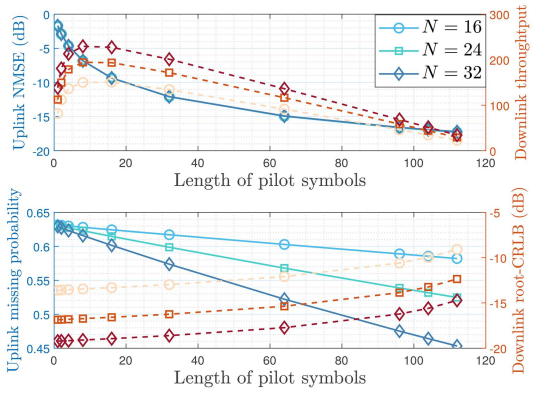

Figure 6 (Color online) Trade-offs between upink and downlink C&S performance as T_u increases versus different N with $N_0 = -80$ dB and $\epsilon_d = 0$ dB.

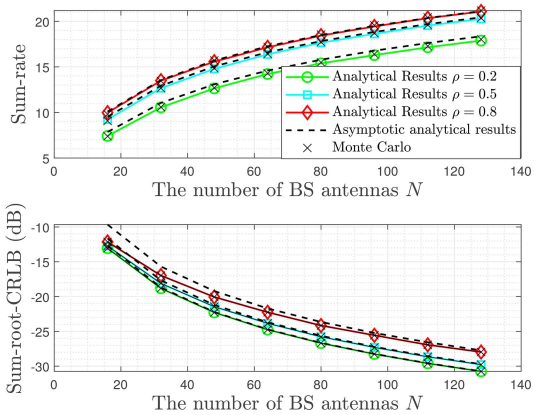

Figure 7 (Color online) Asymptotical behaviors of sum-rate and sum-root-CRLB versus different N and ρ.

In Figure 7, the asymptotic behaviors of sum-rate and sum-root-CRLB are illustrated clearly. It can be observed that asymptotic analytical results closely match the experimental results even at moderate

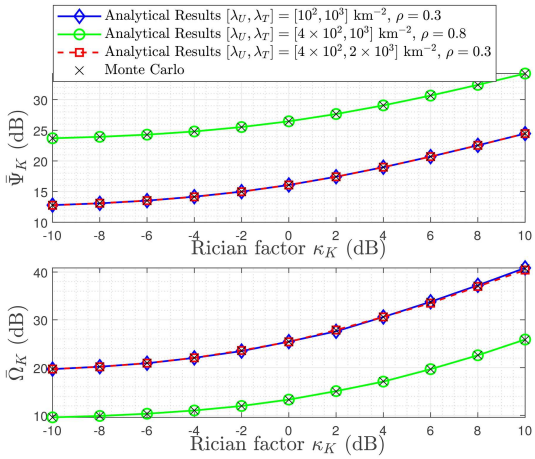

Figure 8 (Color online) Sensing interference ratio and communication enhancement ratio versus different Rician factors.

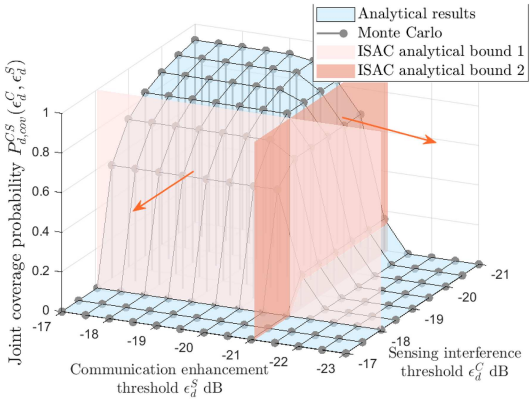

Figure 9 (Color online) Joint coverage probability of downlink ISAC performance versus different communication and sensing thresholds.

values of N, such as $N = 32$. Substantial improvements can be noted in the C&S performance from the increase of N, specifically demonstrating an $\mathcal{O}(\log N)$ gain in the sum-rate and an $\mathcal{O}(N^{-2})$ gain in the sum-root-CRLB, as indicated previously. Moreover, the results reveal that excessively large or small values of ρ lead to deteriorated sensing CRLB and communication rate, respectively. Consequently, a value of $\rho = 0.5$ is recommended to achieve satisfactory ISAC performance.

Figure 8 presents the ergodic ratios $\bar{\Psi}_K$ and $\bar{\Omega}_K$ across all possible locations of CU and ST under varying Rician factors. It can be observed from the overlap of the first and third curves that a linear scaling law between λ_U and λ_T^2 exists, consistent with the uplink process. Additionally, increasing the density and power factor of the CUs reduces the mutual interference $1/\bar{\Psi}_K$ while increasing the mutual benefit $1/\bar{\Omega}_K$. The results also indicate that both $\bar{\Psi}_K$ and $\bar{\Omega}_K$ keep growing with the Rician factor $\kappa_{u,K}$, implying that the mutual interference and benefits diminish as the ISAC channels become more deterministic as noted in Remark 3.

In Figure 9, the joint coverage probability of downlink ISAC performance is demonstrated versus different C&S thresholds, verifying the accuracy of Theorem 2. It also provides two "ISAC analytical bound" surfaces to highlight the fundamental limits of inherent mutual interference and benefits in dual-function coexisting systems. Specifically, these two surfaces are composed of all points satisfying $\epsilon_d^C = \frac{1-\rho}{\rho N(1+\kappa_{u,k})}$ and $\epsilon_d^S = \frac{2\rho}{(1-\rho)N(1+\kappa_{u,k})}$, respectively. It can be observed that the coverage probability within these two bounds drops to zero, further confirming fundamental limits for ISAC systems under coupling effects.

6 Conclusion

In this paper, we have established a comprehensive framework to analyze the fundamental coupling constraints and trade-offs in ISAC systems. In particular, we first investigated the trade-offs through C&S performance regions between the channel estimation error and the successful detection probability in the uplink process, as well as between the transmission rate and CRLB in the downlink process. The theoretical derivations for these metrics provided valuable insights into the scaling laws, asymptotic behaviors, and monotonicity properties of ISAC performance. Additionally, we employed stochastic geometry tools and random matrix theory to characterize the channel coupling effects of large-scale and small-scale fadings on the joint ISAC coverage probabilities. These analyses yield some useful findings into the union bounds for ISAC system designs. Specifically for the uplink process, our results indicated that the channel estimation NMSE cannot be lower than $1 - \frac{2N}{\bar{\epsilon}_u^S}$ when the successful detection probability reaches $Q_1(\sqrt{\bar{\epsilon}_u^S}, \sqrt{2\epsilon_d})$. In the downlink process, we found that the mutual interference and mutual benefit are bounded above by $\frac{1-\rho}{\rho N(1+\kappa)}$ and below by $\frac{2\rho}{(1-\rho)N(1+\kappa)}$, respectively. These derived analytical bounds revealed the fundamental limits for practical ISAC systems imposed by coupling constraints,

which were further validated and illustrated through simulations.

Acknowledgements The work was supported by National Natural Science Foundation of China (Grant Nos. 62331023, 62394292), National Key R&D Program of China (Grant Nos. 2021YFA1000500, 2023YFB2904804), Zhejiang Provincial Science and Technology Plan Project (Grant No. 2024C01033), Zhejiang University Global Partnership Fund, and Fundamental Research Funds for the Central Universities (Grant No. 226-2024-00069). The work of Chau YUEN was supported by the Ministry of Education Tier 2-T2EP50124-0032.

References

1 Liu F, Cui Y, Masouros C, et al. Integrated sensing and communications: toward dual-functional wireless networks for 6G and beyond. IEEE J Sel Areas Commun, 2022, 40: 1728–1767
2 You X H, Wang C-X, Huang J, et al. Towards 6G wireless communication networks: vision, enabling technologies, and new paradigm shifts. Sci China Inf Sci, 2021, 64: 110301
3 Xiao Z Q, Zeng Y. An overview on integrated localization and communication towards 6G. Sci China Inf Sci, 2022, 65: 131301
4 Gui L, Yuan W, Xiao F. CSI-based passive intrusion detection bound estimation in indoor NLoS scenario. Fundamental Res, 2023, 3: 988–996
5 Huang Y. Challenges and opportunities of sub-6 GHz integrated sensing and communications for 5G-advanced and beyond. Chin J Elect, 2024, 33: 323–325
6 Zhou Z C, Liu B, Shen B S, et al. Doppler-resilient waveform design in integrated MIMO radar-communication systems. Sci China Inf Sci, 2024, 67: 112301
7 Wang D, Huang C, He J, et al. Mean field game-based waveform precoding design for mobile crowd integrated sensing, communication, and computation systems. IEEE Trans Wireless Commun, 2024, 23: 10430–10444
8 Xu K, Xia X, Li C, et al. Robust DOA estimation and tracking for integrated sensing and communication massive MIMO OFDM systems. Sci China Inf Sci, 2023, 66: 202302
9 Gan X, Huang C, Yang Z, et al. Bayesian learning for double-RIS aided ISAC systems with superimposed pilots and data. IEEE J Sel Top Signal Process, 2024, 18: 766–781
10 An J, Li H, Ng D W K, et al. Fundamental detection probability vs. achievable rate tradeoff in integrated sensing and communication systems. IEEE Trans Wireless Commun, 2023, 22: 9835–9853
11 Hua H, Han T X, Xu J. MIMO integrated sensing and communication: CRB-rate tradeoff. IEEE Trans Wireless Commun, 2024, 23: 2839–2854
12 Lu S, Liu F, Hanzo L. The degrees-of-freedom in monostatic ISAC channels: NLoS exploitation vs. reduction. IEEE Trans Veh Technol, 2023, 72: 2643–2648
13 Xiong Y, Liu F, Cui Y, et al. On the fundamental tradeoff of integrated sensing and communications under Gaussian channels. IEEE Trans Inform Theor, 2023, 69: 5723–5751
14 Wang X, Yang S, Meng K, et al. On the fundamental trade-offs of time-frequency resource distribution in OFDMA ISAC. 2024. ArXiv:2407.12628
15 Keskin M F, Mojahedian M M, Lacruz J O, et al. Fundamental trade-offs in monostatic ISAC: a holistic investigation towards 6G. 2024. ArXiv:2401.18011
16 Ouyang C, Liu Y, Yang H, et al. Integrated sensing and communications: a mutual information-based framework. IEEE Commun Mag, 2023, 61: 26–32
17 Niu Y, Wei Z, Wang L, et al. Interference management for integrated sensing and communication systems: a survey. IEEE Internet Things J, 2025, 12: 8110–8134
18 Chepuri S P, Shlezinger N, Liu F, et al. Integrated sensing and communications with reconfigurable intelligent surfaces: from signal modeling to processing. IEEE Signal Process Mag, 2024, 40: 41–62
19 Gan X, Huang C, Yang Z, et al. Coverage and rate analysis for integrated sensing and communication networks. IEEE J Sel Areas Commun, 2024, 42: 2213–2227
20 Gan X, Huang C, Yang Z, et al. Modeling and coverage analysis of RIS-assisted integrated sensing and communication networks. IEEE Trans Wireless Commun, 2025. doi: 10.1109/TWC.2025.3550903
21 3GPP. Physical channels and modulation, Release 15. TS 38.211. NR, 2018
22 Zhang R, Zhang H, Xu W, et al. Subarray-based simultaneous beam training for multiuser mmWave massive MIMO systems. IEEE Wireless Commun Lett, 2019, 8: 976–979
23 Iqbal N, Schneider C, Luo J, et al. On the stochastic and deterministic behavior of mmWave channels. In: Proceedings of the European Conference on Antennas and Propagation (EUCAP), Paris, 2017. 1813–1817
24 Kay S M. Fundamentals of Statistical Signal Processing: Estimation Theory. Upper Saddle River: Prentice-Hall, 1993
25 Chalise B K, Amin M G, Himed B. Performance tradeoff in a unified passive radar and communications system. IEEE Signal Process Lett, 2017, 24: 1275–1279
26 Sanguinetti L, Kammoun A, Debbah M. Theoretical performance limits of massive MIMO with uncorrelated rician fading channels. IEEE Trans Commun, 2019, 67: 1939–1955

Appendix A Derivation of the PDF of $\frac{d_{U,K}}{d_{T,K}^2}$

According to the given PDF in (1), we have $f_{d_{U,K}}(x) = \mathrm{e}^{-\lambda_U \pi x^2} \frac{2(\lambda_U \pi x^2)^K}{x(K-1)!}$ and $f_{d_{T,K}}(\bar{x}) = \mathrm{e}^{-\lambda_T \pi \bar{x}^2} \frac{2(\lambda_T \pi \bar{x}^2)^K}{\bar{x}(K-1)!}$.

Let $\bar{Y} = \bar{X}^2$ for $\bar{X} \geqslant 0$ and employ the conversion relationship $f_Y(y) = f_{\bar{X}}(\sqrt{y}) \frac{1}{2\sqrt{y}}$, yielding $f_{d_{T,K}^2}(y) = \mathrm{e}^{-\lambda_T \pi y} \frac{(\lambda_T \pi y)^K}{y(K-1)!}$.

Furthermore, we obtain the PDF of $Z = \frac{X}{Y}$ for $X = d_{U,K}$ and $Y = d_{T,K}^2$, such as

$$\begin{aligned} f_Z(z) &= \int_0^\infty y f_X(yz) f_Y(y) \mathrm{d}y = \int_0^\infty \mathrm{e}^{-\lambda_U \pi y^2 z^2 - \lambda_T \pi y} \frac{2(\lambda_U \pi z^2)^K (\lambda_T \pi)^K y^{3K-1}}{z\left((K-1)!\right)^2} \mathrm{d}y \\ &= \frac{2^{-3K+1} (\lambda_U \pi z^2)^{-\frac{K}{2}} (3K-1)! (\lambda_T \pi)^K}{z\left((K-1)!\right)^2} \mathcal{U}\left(\frac{3K}{2}, \frac{1}{2}, \frac{\lambda_T^2 \pi}{2\lambda_U z^2}\right). \end{aligned} \tag{A1}$$

Appendix B Derivation of the SINR

Substituting the precoding vectors to (15), the SINR expression is written as

$$\gamma_k = \frac{\rho\|\mathbb{E}\{\boldsymbol{h}_k^{\mathrm{H}}\hat{h}_k\}\|^2/\mathbb{E}\{\|\hat{h}_k\|^2\}}{\rho\sum_{i=1}^{K}\mathbb{E}\left\{\|\boldsymbol{h}_k^{\mathrm{H}}\hat{h}_i\|^2\right\}/\mathbb{E}\{\|\hat{h}_i\|^2\} - \rho\|\mathbb{E}\{\boldsymbol{h}_k^{\mathrm{H}}\hat{h}_k\}\|^2/\mathbb{E}\{\|\hat{h}_k\|^2 + (1-\rho)\mathbb{E}\left\{\|\boldsymbol{h}_k^{\mathrm{H}}\boldsymbol{a}_N(\theta_l)\|^2\right\}/N + \frac{P_{d,l}}{N_0}}. \tag{B1}$$

We first compute the term

$$\mathbb{E}\{\|\hat{\boldsymbol{h}}_k\|^2\} = \mu_k\kappa_{u,k}\bar{h}_k^{\mathrm{H}}\bar{h}_k + \phi_k N, \tag{B2}$$

for the equation $\mathbb{E}\{\boldsymbol{x}^{\mathrm{H}}\boldsymbol{A}\boldsymbol{x}\} = \mathrm{tr}\{\boldsymbol{A}(\boldsymbol{\Sigma}+\boldsymbol{\mu}\boldsymbol{\mu}^{\mathrm{H}})\}$ if $\boldsymbol{x}\sim\mathcal{CN}(\boldsymbol{\mu},\boldsymbol{\Sigma})$ for any matrix $\boldsymbol{A}$.

The numerator term is expressed as

$$\|\mathbb{E}\{(\hat{h}_k+\boldsymbol{e}_k)^{\mathrm{H}}\hat{h}_k\}\|^2 = \|\mathbb{E}\{\hat{h}_k^{\mathrm{H}}\hat{h}_k\}\|^2 = \mu_k\kappa_{u,k}\bar{h}_k^{\mathrm{H}}\bar{h}_k + \phi_k N, \tag{B3}$$

where the estimate $\hat{h}_k$ and the error $\boldsymbol{e}_k$ are independent with each other.

The first denominator term for $i\neq k$ as

$$\begin{aligned}\mathbb{E}\left\{\boldsymbol{h}_k^{\mathrm{H}}\hat{h}_i\hat{h}_i^{\mathrm{H}}\boldsymbol{h}_k\right\} &= \mathbb{E}\left\{\mathrm{tr}\left(\hat{h}_i\hat{h}_i^{\mathrm{H}}\left(\mu_k\kappa_{u,k}\bar{h}_k^{\mathrm{H}}\bar{h}_k+\mu_k\boldsymbol{I}\right)\right)\right\} = \mathrm{tr}\left(\left(\mu_i\kappa_{u,i}\bar{h}_i^{\mathrm{H}}\bar{h}_i+\phi_i\boldsymbol{I}\right)\left(\mu_k\kappa_{u,k}\bar{h}_k^{\mathrm{H}}\bar{h}_k+\mu_k\boldsymbol{I}\right)\right)\\ &= \mu_i\mu_k\kappa_{u,i}\kappa_{u,k}\|\bar{h}_k^{\mathrm{H}}\bar{h}_i\|^2 + \mu_i\mu_k\kappa_{u,i}\|\bar{h}_i\|^2 + \phi_i\mu_k\kappa_{u,k}\|\bar{h}_k\|^2 + \phi_i\mu_k N,\end{aligned} \tag{B4}$$

and for $i=k$ as

$$\begin{aligned}\mathbb{E}\left\{\boldsymbol{h}_k^{\mathrm{H}}\hat{h}_k\hat{h}_k^{\mathrm{H}}\boldsymbol{h}_k\right\} &= \mathbb{E}\left\{(\hat{h}_k+\boldsymbol{e}_k)^{\mathrm{H}}\hat{h}_k\hat{h}_k^{\mathrm{H}}(\hat{h}_k+\boldsymbol{e}_k)\right\} = \mathbb{E}\left\{\hat{h}_k^{\mathrm{H}}\hat{h}_k\hat{h}_k^{\mathrm{H}}\hat{h}_k\right\} + \mathbb{E}\left\{\boldsymbol{e}_k^{\mathrm{H}}\hat{h}_k\hat{h}_k^{\mathrm{H}}\boldsymbol{e}_k\right\}\\ &= \phi_k^2 N + 2\mu_k\kappa_{u,k}\phi_k\bar{h}_k^{\mathrm{H}}\bar{h}_k + \left(\phi_k N+\mu_k\kappa_{u,k}\|\bar{h}_k\|^2\right)^2 + \mathrm{tr}\left\{\hat{h}_k\hat{h}_k^{\mathrm{H}}\left(\mu_k-\phi_k\right)\boldsymbol{I}\right\}\\ &= \phi_k\mu_k N + \mu_k\kappa_{u,k}(\mu_k+\phi_k)\|\bar{h}_k\|^2 + \left(\phi_k N+\mu_k\kappa_{u,k}\|\bar{h}_k\|^2\right)^2.\end{aligned} \tag{B5}$$

Then, the sensing interference power can be expressed as

$$\mathbb{E}\left\{\boldsymbol{h}_k^{\mathrm{H}}\boldsymbol{a}_N(\theta_l)\boldsymbol{a}_N^{\mathrm{H}}(\theta_l)\boldsymbol{h}_k\right\} = \mathrm{tr}\left\{\boldsymbol{a}_N(\theta_l)\boldsymbol{a}_N^{\mathrm{H}}(\theta_l)\left(\mu_k\kappa_{u,k}\bar{h}_k\bar{h}_k^{\mathrm{H}}+\mu_k\boldsymbol{I}\right)\right\} = \mu_k\kappa_{u,k}\|\boldsymbol{a}_N^{\mathrm{H}}(\theta_l)\bar{h}_k\|^2 + \mu_k N. \tag{B6}$$

Appendix C Derivation process of $C(\boldsymbol{\theta}_l)$

The data correlation matrix can be expressed as

$$\begin{aligned}\boldsymbol{X}_{d,l}\boldsymbol{X}_{d,l}^{\mathrm{H}} &= P_{d,l}T_d\rho\sum_{k=1}^{K}\sum_{i=1}^{K}\frac{\hat{h}_k\hat{h}_i^{\mathrm{H}}}{\sqrt{\mathbb{E}\{\|\hat{h}_k\|^2\}}\sqrt{\mathbb{E}\{\|\hat{h}_i\|^2\}}} + P_{d,l}T_d(1-\rho)\boldsymbol{a}_N(\theta_l)\boldsymbol{a}_N^{\mathrm{H}}(\theta_l)/N\\ &= P_{d,l}T_d\rho\sum_{k=1}^{K}\sum_{i=1}^{K}\frac{\sqrt{\mu_k\mu_i\kappa_{u,k}\kappa_{u,i}}\bar{h}_k\bar{h}_i^{\mathrm{H}}}{\sqrt{\left(\mu_k\kappa_{u,k}\|\bar{h}_k\|^2+\phi_k N\right)\left(\mu_i\kappa_{u,i}\|\bar{h}_i\|^2+\phi_i N\right)}} + P_{d,l}T_d\rho\sum_{k=1}^{K}\frac{\phi_k\boldsymbol{I}}{\mu_k\kappa_{u,k}\|\bar{h}_k\|^2+\phi_k N}\\ &\quad + P_{d,l}T_d(1-\rho)\boldsymbol{a}_N(\theta_l)\boldsymbol{a}_N^{\mathrm{H}}(\theta_l)/N.\end{aligned} \tag{C1}$$

Then, the term can be written as

$$\begin{aligned}\mathrm{tr}\left(\boldsymbol{A}(\theta_l)\boldsymbol{X}_{d,l}\boldsymbol{X}_{d,l}^{\mathrm{H}}\boldsymbol{A}^{\mathrm{H}}(\theta_l)\right) &= NP_{d,l}\rho T_d\sum_{k=1}^{K}\sum_{i=1}^{K}\frac{\sqrt{\mu_k\mu_i\kappa_{u,k}\kappa_{u,i}}\mathrm{tr}\left(\boldsymbol{a}_N^{\mathrm{H}}(\theta_l)\bar{h}_k\bar{h}_i^{\mathrm{H}}\boldsymbol{a}_N(\theta_l)\right)}{\sqrt{\left(\mu_k\kappa_{u,k}\|\bar{h}_k\|^2+\phi_k N\right)\left(\mu_i\kappa_{u,i}\|\bar{h}_i\|^2+\phi_i N\right)}}\\ &\quad + P_{d,l}\rho T_d\sum_{k=1}^{K}\frac{\phi_k N^2}{\mu_k\kappa_{u,k}\|\bar{h}_k\|^2+\phi_k N} + P_{d,l}(1-\rho)T_d N^2.\end{aligned} \tag{C2}$$

Besides, the equation that is often used can be expressed as

$$\begin{aligned}\boldsymbol{a}_N^{\mathrm{H}}(\theta_l)\breve{a}_N(\theta_l) &= \frac{N(N-1)}{2}\mathrm{j}\pi\cos(\theta_l),\ \breve{a}_N^{\mathrm{H}}(\theta_l)\boldsymbol{a}_N(\theta_l)\\ &= -\frac{N(N-1)}{2}\mathrm{j}\pi\cos(\theta_l),\ \breve{a}_N^{\mathrm{H}}(\theta_l)\breve{a}_N(\theta_l) = \frac{N(N-1)(2N-1)}{6}\pi^2\cos^2(\theta_l).\end{aligned} \tag{C3}$$

The second term is written as

$$\begin{aligned}&\mathrm{tr}\left(\boldsymbol{A}(\theta_l)\boldsymbol{X}_{d,l}\boldsymbol{X}_{d,l}^{\mathrm{H}}\breve{A}^{\mathrm{H}}(\theta_l)\right) = \mathrm{tr}\left(\boldsymbol{a}_N(\theta_l)\boldsymbol{a}_N^{\mathrm{H}}(\theta_l)\boldsymbol{X}_{d,l}\boldsymbol{X}_{d,l}^{\mathrm{H}}\breve{a}_N(\theta_l)\boldsymbol{a}_N^{\mathrm{H}}(\theta_l)\right) + \mathrm{tr}\left(\boldsymbol{a}_N(\theta_l)\boldsymbol{a}_N^{\mathrm{H}}(\theta_l)\boldsymbol{X}_{d,l}\boldsymbol{X}_{d,l}^{\mathrm{H}}\boldsymbol{a}_N(\theta_l)\breve{a}_N^{\mathrm{H}}(\theta_l)\right)\\ &= P_{d,l}\rho T_d\sum_{k=1}^{K}\sum_{i=1}^{K}\frac{\sqrt{\mu_k\mu_i\kappa_{u,k}\kappa_{u,i}}\left(N\mathrm{tr}\left(\boldsymbol{a}_N^{\mathrm{H}}(\theta_l)\bar{h}_k\bar{h}_i^{\mathrm{H}}\breve{a}_N(\theta_l)\right) - \frac{N(N-1)}{2}j\pi\cos(\theta_l)\mathrm{tr}\left(\boldsymbol{a}_N^{\mathrm{H}}(\theta_l)\bar{h}_k\bar{h}_i^{\mathrm{H}}\boldsymbol{a}_N(\theta_l)\right)\right)}{\sqrt{\left(\mu_k\kappa_{u,k}\|\bar{h}_k\|^2+\phi_k N\right)\left(\mu_i\kappa_{u,i}\|\bar{h}_i\|^2+\phi_i N\right)}}.\end{aligned} \tag{C4}$$

The third term can be computed by

$$\begin{aligned}
&\mathrm{tr}\left(\breve{A}(\theta_l)\boldsymbol{X}_{d,l}\boldsymbol{X}_{d,l}^{\mathrm{H}}\breve{A}^{\mathrm{H}}(\theta_l)\right)=\mathrm{tr}\left(\breve{\boldsymbol{a}}_N(\theta_l)\boldsymbol{a}_N^{\mathrm{H}}(\theta_l)\boldsymbol{X}_{d,l}\boldsymbol{X}_{d,l}^{\mathrm{H}}\breve{\boldsymbol{a}}_N(\theta_l)\boldsymbol{a}_N^{\mathrm{H}}(\theta_l)\right)+\mathrm{tr}\left(\breve{\boldsymbol{a}}_N(\theta_l)\boldsymbol{a}_N^{\mathrm{H}}(\theta_l)\boldsymbol{X}_{d,l}\boldsymbol{X}_{d,l}^{\mathrm{H}}\boldsymbol{a}_N(\theta_l)\breve{\boldsymbol{a}}_N^{\mathrm{H}}(\theta_l)\right)\\
&+\mathrm{tr}\left(\boldsymbol{a}_N(\theta_l)\breve{\boldsymbol{a}}_N^{\mathrm{H}}(\theta_l)\boldsymbol{X}_{d,l}\boldsymbol{X}_{d,l}^{\mathrm{H}}\breve{\boldsymbol{a}}_N(\theta_l)\boldsymbol{a}_N^{\mathrm{H}}(\theta_l)\right)+\mathrm{tr}\left(\boldsymbol{a}_N(\theta_l)\breve{\boldsymbol{a}}_N^{\mathrm{H}}(\theta_l)\boldsymbol{X}_{d,l}\boldsymbol{X}_{d,l}^{\mathrm{H}}\boldsymbol{a}_N(\theta_l)\breve{\boldsymbol{a}}_N^{\mathrm{H}}(\theta_l)\right)=P_{d,l}\rho T_d\\
&\cdot\sum_{k=1}^{K}\sum_{i=1}^{K}\frac{\sqrt{\mu_k\mu_i\kappa_{u,k}\kappa_{u,i}}\left(\frac{N(N-1)}{2}\mathrm{j}\pi\cos(\theta_l)\mathrm{tr}\left(\boldsymbol{a}_N^{\mathrm{H}}(\theta_l)\bar{h}_k\bar{h}_i^{\mathrm{H}}\breve{\boldsymbol{a}}_N(\theta_l)\right)+\frac{N(N-1)(2N-1)}{6}\pi^2\cos^2(\theta_l)\mathrm{tr}\left(\boldsymbol{a}_N^{\mathrm{H}}(\theta_l)\bar{h}_k\bar{h}_i^{\mathrm{H}}\boldsymbol{a}_N(\theta_l)\right)\right)}{\sqrt{\left(\mu_k\kappa_{u,k}\|\bar{h}_k\|^2+\phi_kN\right)\left(\mu_i\kappa_{u,i}\|\bar{h}_i\|^2+\phi_iN\right)}}\\
&\cdot\frac{\sqrt{\mu_k\mu_i\kappa_{u,k}\kappa_{u,i}}\left(N\mathrm{tr}\left(\breve{\boldsymbol{a}}_N^{\mathrm{H}}(\theta_l)\bar{h}_k\bar{h}_i^{\mathrm{H}}\breve{\boldsymbol{a}}_N(\theta_l)\right)-\frac{N(N-1)}{2}\mathrm{j}\pi\cos(\theta_l)\mathrm{tr}\left(\breve{\boldsymbol{a}}_N^{\mathrm{H}}(\theta_l)\bar{h}_k\bar{h}_i^{\mathrm{H}}\boldsymbol{a}_N(\theta_l)\right)\right)}{\sqrt{\left(\mu_k\kappa_{u,k}\|\bar{h}_k\|^2+\phi_kN\right)\left(\mu_i\kappa_{u,i}\|\bar{h}_i\|^2+\phi_iN\right)}}\\
&+P_{d,l}\rho T_d\frac{N^2(N^2-1)}{6}\pi^2\cos^2(\theta_l)\sum_{k=1}^{K}\frac{\phi_k}{\mu_k\kappa_{u,k}\|\bar{h}_k\|^2+\phi_kN}+P_{d,l}(1-\rho)T_d\frac{N^2(N^2-1)}{12}\pi^2\cos^2(\theta_l).
\end{aligned}\tag{C5}$$

Appendix D Derivation of $\bar{\boldsymbol{C}}(\boldsymbol{\theta_l})$

For the infinite antenna systems, we have

$$\Pi_{AA}^{l}\overset{N\to\infty}{\longrightarrow}\rho\sum_{k=1}^{K}\frac{\phi_kN^2}{\mu_k\kappa_{u,k}+\phi_k}+(1-\rho)N^2.\tag{D1}$$

Then, we investigate the asympototic behavior of $\boldsymbol{a}_N^{\mathrm{H}}(\varphi_k)\breve{\boldsymbol{a}}_N(\theta_l)$ as

$$\begin{aligned}
\boldsymbol{a}_N^{\mathrm{H}}(\varphi_k)\breve{\boldsymbol{a}}_N(\theta_l)&=\sum_{n=1}^{N-1}n\mathrm{j}\pi\cos(\theta_l)\mathrm{e}^{n\mathrm{j}\pi\Delta s}\\
&=\frac{\mathrm{j}\pi\cos(\theta_l)}{\left(\mathrm{e}^{\mathrm{j}\pi\Delta s}-1\right)^2}\left[N\left(\mathrm{e}^{\mathrm{j}\pi(N+1)\Delta s}-\mathrm{e}^{\mathrm{j}\pi N\Delta s}\right)-\mathrm{e}^{\mathrm{j}\pi(N+1)\Delta s}+\mathrm{e}^{\mathrm{j}\pi\Delta s}\right]\\
&=\frac{\mathrm{j}\pi\cos(\theta_l)N}{\mathrm{e}^{\mathrm{j}\pi\Delta s}-1}\mathrm{e}^{\mathrm{j}\pi N\Delta s}+\frac{\mathrm{j}\pi\cos(\theta_l)}{1-\mathrm{e}^{\mathrm{j}\pi\Delta s}}\mathrm{e}^{\mathrm{j}\pi\Delta s}\frac{1-\mathrm{e}^{\mathrm{j}\pi N\Delta s}}{1-\mathrm{e}^{\mathrm{j}\pi\Delta s}}\\
&=\frac{\pi\cos(\theta_l)N}{2\sin(\frac{\pi}{2}\Delta s)}\mathrm{e}^{\mathrm{j}\pi(N-\frac{1}{2})\Delta s}-\frac{\pi\cos(\theta_l)}{2\sin(\frac{\pi}{2}\Delta s)}\mathrm{e}^{\mathrm{j}\pi\frac{N}{2}\Delta s}\frac{\sin(\frac{\pi N\Delta s}{2})}{\sin(\frac{\pi\Delta s}{2})}.
\end{aligned}\tag{D2}$$

Since $\sin(\frac{\pi}{2}N_\epsilon)\leqslant|\sin(\frac{\pi}{2}\Delta s)|\leqslant 1$, we have

$$\frac{\pi\cos(\theta_l)N}{2\sin(\frac{\pi}{2}\Delta s)}\mathrm{e}^{\mathrm{j}\pi(N-\frac{1}{2})\Delta s}/N^2\overset{N\to\infty}{\longrightarrow}0.\tag{D3}$$

Besides, as for $N_\epsilon>\frac{2}{N}$, it can be derived $\frac{\sin(\frac{\pi N\Delta s}{2})}{\sin(\frac{\pi\Delta s}{2})}/N\overset{N\to\infty}{\longrightarrow}0$ and further

$$\frac{\pi\cos(\theta_l)}{2\sin(\frac{\pi}{2}\Delta s)}\mathrm{e}^{\mathrm{j}\pi\frac{N}{2}\Delta s}\frac{\sin(\frac{\pi N\Delta s}{2})}{\sin(\frac{\pi\Delta s}{2})}/N^2\overset{N\to\infty}{\longrightarrow}0.\tag{D4}$$

Hence, combining the asympototic behavior in (D3) and (D4), we have

$$\boldsymbol{a}_N^{\mathrm{H}}(\varphi_k)\breve{\boldsymbol{a}}_N(\theta_l)/N^2\overset{N\to\infty}{\longrightarrow}0.\tag{D5}$$

Then, we have

$$\Pi_{\breve{A}\breve{A}}^{l}\overset{N\to\infty}{\longrightarrow}\rho\frac{N^2(N^2-1)}{6}\pi^2\cos^2(\theta_l)\sum_{k=1}^{K}\frac{\phi_k}{\mu_k\kappa_{u,k}+\phi_k}+(1-\rho)\frac{N^2(N^2-1)}{12}\pi^2\cos^2(\theta_l).\tag{D6}$$

As for the term $\Pi_{A\breve{A}}^{\mathrm{square}}$, we have

$$\mathrm{tr}\left(\boldsymbol{a}_N^{\mathrm{H}}(\theta_l)\bar{h}_k\bar{h}_i^{\mathrm{H}}\breve{\boldsymbol{a}}_N(\theta_l)\right)/N^3\overset{N\to\infty}{\longrightarrow}0,\tag{D7}$$

and

$$\mathrm{tr}\left(\boldsymbol{a}_N^{\mathrm{H}}(\theta_l)\bar{h}_k\bar{h}_i^{\mathrm{H}}\boldsymbol{a}_N(\theta_l)\right)/N^2\overset{N\to\infty}{\longrightarrow}0,\tag{D8}$$

which deduce that

$$\Pi_{A\breve{A}}^{l,\mathrm{square}}/N^6\overset{N\to\infty}{\longrightarrow}0.\tag{D9}$$

Combining the asympototic behaviors in (D1), (D6), and (D9), we have

$$\Pi_{\breve{A}\breve{A}}^{l}-\frac{\Pi_{A\breve{A}}^{l,\mathrm{square}}}{\Pi_{AA}^{l}}\overset{N\to\infty}{\longrightarrow}\Pi_{\breve{A}\breve{A}}^{l}.\tag{D10}$$

Appendix E Derivation process of $\bar{\Psi}_k$ and $\bar{\Omega}_k$

The statistical communication enhancement ratio can be expressed as

$$\begin{aligned}
\bar{\Omega}_k &= \mathbb{E}_{\mu_k,\beta_{t,k}}\left\{\frac{(1-\rho)N}{2\rho}\left(\kappa_{u,K}+1+\frac{\kappa_{u,K}(P_{T,k}N\beta_{t,k}+N_0)}{P_{U,k}\mu_k}\right)\right\}\\
&= \frac{(1-\rho)N}{2\rho}(\kappa_{u,K}+1)+\mathbb{E}_{\beta_{t,k}}\left\{\frac{(1-\rho)N}{2\rho}\kappa_{u,K}(P_{T,k}N\beta_{t,k}+N_0)\int_0^\infty \frac{1}{P_{U,k}C_0 r_U^{-\alpha}}\mathrm{e}^{-\lambda_U\pi r_U^2}\frac{2(\lambda_U\pi r_U^2)^k}{r_U(k-1)!}\mathrm{d}r_U\right\}\\
&= \frac{(1-\rho)N}{2\rho}(\kappa_{u,k}+1)+\frac{(1-\rho)N}{2\rho}(\lambda_U\pi)^{-\frac{\alpha}{2}}\frac{\kappa_{u,k}(1+\kappa_{u,k})\Gamma(k+\frac{\alpha}{2})}{P_{U,k}\Gamma(k)C_0}\left(N_0+P_{T,k}NC_0(r_T)^{-2\alpha}\mathrm{e}^{-\lambda_T\pi r_T^2}\frac{2(\lambda_T\pi r_T^2)^k}{r_T(k-1)!}\mathrm{d}r_T\right)\\
&= \frac{(1-\rho)N}{2\rho}(\kappa_{u,k}+1)+\frac{(1-\rho)N}{2\rho}(\lambda_U\pi)^{-\frac{\alpha}{2}}\frac{\kappa_{u,k}(1+\kappa_{u,k})\Gamma(k+\frac{\alpha}{2})}{P_{U,k}\Gamma(k)}\left(\frac{N_0}{C_0}+(\lambda_T\pi)^{\alpha}P_{T,k}N\frac{\Gamma(k-\alpha)}{\Gamma(k)}\right).
\end{aligned} \tag{E1}$$

Besides, the statistical Ψ_k can be expressed as

$$\begin{aligned}
\bar{\Psi}_k &= \frac{\rho N\kappa_{u,k}}{1-\rho}+\frac{\rho N}{1-\rho}\cdot\int_0^\infty\left(\frac{P_{U,k}C_0 r_U^{-2}}{P_{U,k}C_0 r_U^{-2}+(1+\kappa_{u,k})P_T N\beta_{t,k}+(1+\kappa_{u,k})N_0}\right)\mathrm{e}^{-\lambda_U\pi r_U^2}\frac{2(\lambda_U\pi r_U^2)^k}{r_U(k-1)!}\mathrm{d}r_U\\
&\overset{\text{a}}{=} \frac{\rho N\kappa_{u,k}}{(1-\rho)(k-1)!}+\frac{2\rho N(\lambda_U\pi)^k}{1-\rho}\cdot\int_0^\infty\left(\frac{P_{U,k}C_0 u^{k-1}}{P_{U,k}C_0+u(1+\kappa_{u,k})\left(P_T N\beta_{t,k}+N_0\right)}\right)\mathrm{e}^{-\lambda_U\pi u}\mathrm{d}r_U\\
&= \frac{\rho N\kappa_{u,k}}{1-\rho}+\frac{\rho N}{(1-\rho)}\left(\frac{\lambda_U\pi P_{U,k}C_0}{(1+\kappa_{u,k})\left(P_T N\beta_{t,k}+N_0\right)}\right)^k E_k\left(\frac{\lambda_U\pi P_{U,k}C_0}{(1+\kappa_{u,k})\left(P_T N\beta_{t,k}+N_0\right)}\right)\\
&\quad\cdot\exp\left(\frac{\lambda_U\pi P_{U,k}C_0}{(1+\kappa_{u,k})\left(P_T N\beta_{t,k}+N_0\right)}\right),
\end{aligned} \tag{E2}$$

where Eq. (a) is obtained by $u=r_U^2$ and then using Laplace transform of $\frac{P_{U,k}C_0u^{k-1}}{P_{U,k}C_0+u(1+\kappa_{u,k})\left(P_T N\beta_{t,k}+N_0\right)}$.